A Section 508–conformant HTML version of this article is available at https://doi.org/10.1289/EHP9505.

Role of OCT3 and DRP1 in the Transport of Paraquat in Astrocytes: A Mouse Study

Sida Han,[1] Yiwei Feng,[1*] Min Guo,[1*] Yining Hao,[1] Jian Sun,[1] Yichen Zhao,[2] Qiang Dong,[3,4,5] Yanxin Zhao,[2] and Mei Cui[1,5]*

[1]Department of Neurology, Huashan Hospital, Fudan University, Shanghai, China
[2]Department of Neurology, Tenth People's Hospital, Tongji University, Shanghai, China
[3]Department of Neurology, Huashan Hospital, State Key Laboratory of Medical Neurobiology, Fudan University, Shanghai, China
[4]Ministry of Education (MOE) Frontiers Center for Brain Science, Fudan University, Shanghai, China
[5]National Center for Neurological Disorders, Huashan Hospital, Fudan University, Shanghai, China

Background: Paraquat (PQ) is a pesticide, exposure to which has been associated with an increased risk of Parkinson's disease; however, PQ transport mechanisms in the brain are still unclear. Our previous studies indicated that the organic cation transporter 3 (OCT3) expressed on astrocytes could uptake PQ and protect the dopaminergic (DA) neurons from a higher level of extracellular PQ. At present, it is unknown how OCT3 levels are altered during chronic PQ exposure or aging, nor is it clear how the compensatory mechanisms are triggered by OCT3 deficiency. Dynamic related protein 1 (DRP1) was previously reported to ameliorate the loss of neurons during Parkinson's disease. Nowadays, mounting studies have revealed the functions of astrocyte DRP1, prompting us to hypothesize that DRP1 could regulate the PQ transport capacity of astrocytes.

Objectives: The present study aimed to further explore PQ transport mechanisms in the nigrostriatal system and identify pathways involved in extracellular PQ clearance.

Methods: Models of PQ-induced neurodegeneration were established by intraperitoneal (i.p.) injection of PQ in wild-type (WT) and organic cation transporter-3–deficient ($Oct3^{-/-}$) mice. DRP1 knockdown was achieved by viral tools *in vivo* and small interfering RNA (siRNA) *in vitro*. Extracellular PQ was detected by *in vivo* microdialysis. *In vitro* transport assays were used to directly observe the functions of different transporters. PQ-induced neurotoxicity was evaluated by tyrosine hydroxylase immunohistochemistry, *in vivo* microdialysis for striatal DA and behavior tests. Western blotting analysis or immunofluorescence was used to evaluate the expression levels and locations of proteins *in vitro* or *in vivo*.

Results: Older mice and those chronically exposed to PQ had a lower expression of brain OCT3 and, following exposure to a 10-mg/kg i.p. PQ^{2+} loading dose, a higher concentration of extracellular PQ. DRP1 levels were higher in astrocytes and neurons of WT and $Oct3^{-/-}$ mice after chronic exposure to PQ; this was supported by finding higher levels of DRP1 after PQ treatment of dopamine transporter-expressing neurons with and without OCT3 inhibition and in primary astrocytes of WT and $Oct3^{-/-}$ mice. Selective astrocyte DRP1 knockdown ameliorated the PQ^{2+}-induced neurotoxicity in $Oct3^{-/-}$ mice but not in WT mice. GL261 astrocytes with siRNA-mediated DRP1 knockdown had a higher expression of alanine–serine–cysteine transporter 2 (ASCT2), and transport studies suggest that extracellular PQ was transported into astrocytes by ASCT2 when OCT3 was absent.

Discussion: The present study mainly focused on the transport mechanisms of PQ between the dopaminergic neurons and astrocytes. Lower OCT3 levels were found in the older or chronically PQ-treated mice. Astrocytes with DRP1 inhibition (by viral tools or mitochondrial division inhibitor-1) had higher levels of ASCT2, which we hypothesize served as an alternative transporter to remove extracellular PQ when OCT3 was deficient. In summary, our data suggest that OCT3, ASCT2 located on astrocytes and the dopamine transporter located on DA terminals may function in a concerted manner to mediate striatal DA terminal damage in PQ-induced neurotoxicity. https://doi.org/10.1289/EHP9505

Introduction

Paraquat [1,1′-dimethyl-4,4′-bipyridinium dichloride (PQ)], as one of the widely used broad-spectrum cationic herbicides,[1–3] has been associated with a variety of toxicities, including pulmonary,[4] neuro-,[5] and nephrotoxicity.[6] Experimental and epidemiological studies have shown that PQ is closely related to Parkinson's disease (PD) risk.[7–9] In experimental studies, PQ has been reported to impact mitochondrial functions and to produce reactive oxygen species (ROS),[10–13] causing loss of dopamine neurons, poor locomotor performance, and synuclein aggregation.[14–17] As reported previously in mouse studies, PQ^{2+} induces apoptosis of dopaminergic (DA) neurons in the substantia nigra, but because of compensatory striatal sprouting in the remaining neurons, the striatum is spared.[18–20] However, when organic cation transporter-3 (OCT3), a bidirectional transporter highly expressed in astrocytes, is deleted, PQ^{2+} could induce significant loss in both DA neurons and terminals in the nigrostriatal system.[19,21]

Interestingly, mouse and cell studies have reported that PQ^{2+} can be reduced to PQ^{+} by enzymes such as nicotinamide adenine dinucleotide phosphate (NADPH)-oxidase,[19] and microglia in the brain have been suggested to be the critical cell type for PQ toxicity.[22,23] In human and rodent studies, PQ^{+} has been reported to be the substrate for both dopamine transporter (DAT) and OCT3.[24,25] As reported in mouse and cell studies, because OCT3 has a higher affinity for PQ^{+} than DAT, extracellular PQ^{+} can be readily cleared by OCT3 located on astrocytes, leaving less PQ available for DAT-mediated transport into striatal terminals.[19,21] Overall, these studies focused on the transport process of PQ in the rodent nigrostriatal system, where OCT3 serves as a critical regulator. However, little is known about the changes in transport functions of OCT3 during aging or chronic PQ exposure, nor is it clear whether compensatory mechanisms prevail during OCT3 dysfunction.

*These authors contributed equally to this work.
Address correspondence to Mei Cui, Department of Neurology, Huashan Hospital, Fudan University, No.12 Middle Wulumuqi Rd., Shanghai 200040 China. Telephone: 021-52888164. Email: cuimei@fudan.edu.cn. Or, Yanxin Zhao, Department of Neurology, Shanghai Tenth People's Hospital, Tongji University School of Medicine, Shanghai 200072 China. Telephone: 021-52888164. Email: zhao_yanxin@126.com. Or, Qiang Dong, Department of Neurology, Huashan Hospital, State Key Laboratory of Medical Neurobiology and MOE Frontiers Center for Brain Science, Fudan University, No. 12 Middle Wulumuqi Road, Shanghai 200040 China. Telephone: 021-52888160. E-mail: dong_qiang@fudan.edu.cn

Supplemental Material is available online (https://doi.org/10.1289/EHP9505).
The authors declare they have no actual or potential competing financial interests.
Received 15 April 2021; Revised 24 March 2022; Accepted 31 March 2022; Published 5 May 2022.

Dynamin-related protein 1 (DRP1) is acknowledged as an inducer of mitochondrial fragmentation,[26] and neural DRP1 inhibition can ameliorate neurodegeneration in rodents.[26–28] However, to the best of our knowledge, little attention has been paid to astrocyte DRP1. Recently, DRP1 inhibition has been found to impact astrocyte function in mouse and cell studies,[29,30] which prompted us to hypothesize on the potential effect of astrocyte DRP1 on PQ-induced neurotoxicity, especially the clearance process of extracellular PQ mediated by astrocytes.

In the present study, PQ^{2+}-induced neurodegeneration was modeled in C57BL/6 mice by intraperitoneal (i.p.) injection of PQ^{2+}, commonly used in other PD-related studies.[18,31–34] To further understand the mechanisms of PQ-induced neurotoxicity, the loss of nigral DA neurons and striatal terminals, the ability of synapses to release DA, and animal behaviors in both $Oct3^{-/-}$ and wild-type (WT) mice were evaluated by immunohistochemistry (IHC), *in vivo* microdialysis, and behavior tests, respectively. *In vitro* transporter assays were conducted to directly evaluate the transporting capacity of different PQ transporters, including OCT3 and ASCT2, another monovalent cation transporter expressed in astrocytes that serve as an alternative transporter to remove extracellular PQ when OCT3 is deficient. These results provide a better understanding of the transporting processes of PQ in the rodent brain.

Materials and Methods

Animals

Eight-week-old male C57BL/6 (WT) mice were purchased from Beijing Vital River Laboratory Animal Technology Co., Ltd. After arrival, the WT mice were raised for 2 wk without any treatment to adapt to the environment and avoid stress. $Oct3^{-/-}$ mice were originally generated by Zwart et al.[35] and kindly gifted from K. Tieu (Florida International University). The animals were housed at $23 \pm 1°C$, $55 \pm 5\%$ humidity with a 12-h light/dark cycle (lights on between 0700 and 1900 hours). Water and standard chow were provided *ad libitum*. $Oct3^{-/-}$ mice were bred in an animal platform, at the Institute of Neurology, Huashan Hospital, Fudan University. Eight- to twelve-wk-old homozygous $Oct3^{-/-}$ breeders were mated, and once the vaginal embolus was found, the pregnant female mice were raised separately from other mice, until they gave birth to the newborns and fed for 4 wk. Mouse tail tissue was taken for genotyping by quantitative polymerase chain reaction (qPCR). After genotyping, male $Oct3^{-/-}$ mice were used for experiments. The study was performed with the approval of the Institutional Animal Care and Use Committee of Fudan University. The experiments were performed according to the National Institute of Health *Guide for the Care and Use of Laboratory Animals*.[36]

Animal Genotyping

Mouse tail tissue was cut and ground in Trizol (Takara; Cat. No. D9108A), 0.5 mL for each sample, and the process of RNA isolation was conducted on ice. One-half milliliter of chloroform was added to each tube and the tube was violently shaken for 30 s, followed by allowing the sample to stand for 10 min, until the liquid was layered. The sample was centrifuged at $12,000 \times g$ 15 min at 4°C. The supernatant was collected into another tube and gently mixed with 0.5 mL of isopropyl alcohol, followed by gentle shaking and then allowed to stand for 15 min. The tube was centrifuged again at $12,000 \times g$ 15 min at 4°C. The supernatant was removed and 1 mL of 75% ethanol was added into the tube. After gentle shaking, the tube was centrifuged at $7,500 \times g$ for 10 min at 4°C. The pellet was collected and dissolved in 20 μL of diethyl pyrocarbonate (DEPC) water. The sample was prepared for reverse transcription, and the Takara Reverse Transcription Kit (Cat. No. RR036A) was used. To each 500-ng RNA sample, 2 μL of $5 \times$ PrimeScript RT Master Mix and an appropriate volume of DEPC water was mixed to yield 10 μL. The thermal cycle parameters were as follows: 37°C × 15 min → 85°C × 15 s → 4°C∞. After reverse transcription, the samples were stored at 4°C and prepared for qPCR. The Takara qPCR kit (Cat. No. RR420A) was used. The system included 2 μL of complementary DNA (cDNA), 10 μL of TB Green, 0.8 μL each of forward and backward primer, 6 μL of DEPC water, and 0.4 μL of ROX Reference Dye. The sequences of the *oct3* primers were as follows: forward 5′-GCCCGGAGCTCTCTTAATCC-3′; reverse 5′-CTCAGCCACGGTATCCCTTC-3′. The samples were added into 96-well plates. The Thermo Fisher Quant Studio5 Real-Time PCR system was used, and the thermal cycle parameters were as follows: stage 1: 95°C 30 s, 1 cycle; stage 2: 95°C 5 s → 60°C 30 s, 40 cycles; stage 3: 95°C 5 s → 60°C 60 s, 1 cycle; stage 4: 95°C → room temperature, continuous.

PQ^{2+} Preparations and Animal Treatments

PQ^{2+} (Chemical Abstracts Services No. 75365-73-0; Sigma-Aldrich; Cat. No. 36541) was diluted in phosphate-buffered saline (PBS) to a 2-mg/mL concentration, and both WT and $Oct3^{-/-}$ mice received PQ^{2+} by i.p. injection. (The extracellular PQ^{2+} concentration was measured in this study and it could not be achieved by any other method, including inhalation or gavage.) The dose (10 mg/kg) was used in this study based on the National Health Commission of China standard, which indicated that the permissible concentration–time-weighted average (PC-TWA) allowed for PQ is $0.5\ mg/m^3$. Considering that the daily respiratory volume of a person is estimated as $10–20\ m^3$, and the body weight of a person is estimated to be 50 kg, 0.1–0.2 mg/kg of PQ was allowed for a human. The dose for a mouse might be 10–20 mg/kg/d according to the uncertainty coefficient (100). In the present study, a 10-mg/kg PQ dose was used.[30]

As shown in Figure S1, the mice were treated as follows: *a*) For the PQ^{2+} chronic treatment (PQ^{2+}-CT), the mice received PQ^{2+} injection (i.p., 10 mg/kg) every 2 d, with a total of 10 injections in 20 d. *b*) For the PBS treatment (PBS), the mice received the same volume of PBS (i.p.) every 2 d, with a total of 10 injections in 20 d. Then, the mice were allowed a 1-wk wash-out period. After the wash-out period, the mice were used for behavioral tests, followed by IHC ($n = 10$ mice per group) or *in vivo* microdialysis ($n = 5$ mice per group) to evaluate DA release (Figure S1A,B).

To evaluate the clearance capacity of the loading PQ^{2+} in the brains of the mice, a second cohort of WT and $Oct3^{-/-}$ mice with or without adeno-associated virus (AAV) injection ($n = 5$ mice per group) underwent PBS or PQ^{2+}-CT. After a 1-wk wash-out period, all groups received a loading dose injection of PQ^{2+} [i.p., 10 mg/kg; PQ^{2+} loading treatment (PQ^{2+}-LT)]. Twenty-four hours after PQ^{2+}-LT, extracellular PQ^{2+} was detected by *in vivo* microdialysis (Figure S1C).

To assess the cerebral expression level of OCT3 in mice of different ages, WT mice were raised to 10, 24, or 48 wk of age before PQ^{2+}-CT or PBS treatment ($n = 5$ mice per group). After the 1-wk wash-out period, all the mice underwent PQ^{2+}-LT. Then 24 h later, *in vivo* microdialysis was used to evaluate the extracellular PQ^{2+} concentration in the brain. Subsequently, the mice were euthanized by isoflurane (RWD; Cat. No. R-510-22-16), and the brain tissues were harvested for OCT3 detection by Western blotting (Figure S1D).

Cell Culture

The HEK293 (Cat. No. h242), GL261 (Cat. No. m063), and Neuro-2a (N_2a; Cat. No. m040) cell lines were purchased from iCell Co., Ltd. The cells were cultured in Dulbecco's Modified

Eagle Medium (DMEM; Sangon Biotech; Cat. No. H531FA0004) mixed with 10% vol/vol fetal bovine serum (FBS; Gibco; Cat. No. 10100147) and 1% vol/vol penicillin–streptomycin (P/S; Gibco; Cat. No. 2289321) solution. The incubator environment was maintained at 37°C and 5% carbon dioxide (CO_2). The cells were subcultured until a confluence of 80% was attained. The cells were then maintained in 10-cm dishes (Corning; Cat. No. 430167). The cells were plated into 6- (Corning; Cat. No. 3516) or 24-well (Corning; Cat. No. 3524) dishes for plasmid transferring, PQ transporting experiments, and Western blotting.

Construction of AAV Tools and Stereotactic Injection

Interfering microRNA (miRNA) to block DRP1 (sequence: 5′-CGTTGTCAACCTGACACTTGT-3′) was constructed and purchased from Shanghai Taitool Bioscience Co., Ltd.; Cat. No. DNM1L-RNAi 33461-1. Scramble miRNA (sequence: 5′-AAATGTACTGCGCGTGGAGAC-3′, Shanghai Taitool Bioscience Co., Ltd.; Cat. No. NO.1) was used as the negative control. Both miRNAs were stored as freeze-dried powder at −80°C and dissolved in DEPC water to yield a 1-μg/μL solution before use.

To test the knockdown efficiency, miRNA was co-transferred into HEK293 cells with *Drp1-egfp* (Shanghai Bioegene Co., Ltd.; Cat. No. BIOE-PL-OE19). In detail, 0.5 μg of miRNA and 0.5 μg of *Drp1-egfp* were mixed and dissolved into 0.5 mL of DMEM. Three microliters of lipofectamine 2000 (Thermo; Cat. No. 11668019) was added into another 0.5 mL of DMEM. After 5 min of equilibration, the above two solutions were mixed and allowed to stand for 20 min, after which the mixture was added onto HEK293 cells. The cells were cultured in 6-well plates, reaching a confluence of 50% before transferring. After 48 h of incubation, the cells were gently scraped off and resuspended into culture medium (2 mL per well). One-half milliliter of cell suspension was added onto a cell-slide placed into a well of a 24-well plate. After 24 h, cells had become attached to the slide. Four percent paraformaldehyde (PFA) was then gently added onto the slide, and it was incubated for 20 min. Then the cells on the slide were observed under a fluorescence microscope (Olympus DP72) for detections of enhanced green fluorescent protein (eGFP) fluorescence intensity, which was analyzed using ImageJ software (Wayne Rasband, National Institutes of Health, Bethesda, MD). The other 1.5 mL of the cell suspension was centrifuged at 1,000 rpm for 5 min at 4°C to harvest the pellet. One hundred microliters of radio-immunoprecipitation assay (RIPA) buffer was added onto the pellet. After quantifying the protein (as described below), the DRP1 level was detected by Western blotting (both experiments were repeated three times with three replicate wells each time).

Then, the miRNA was cloned onto an astrocyte-specific RNA interference (RNAi) vector [pAAV2-gfaABC1D-mCherry-miRNA-WPRE-pA; Cat. No. AI004; Shanghai Taitool Bioscience Co., Ltd. gfaABC1D: a truncated 681-bp glial fibrillary acidic protein (GFAP) promoter] and a neuron-specific RNAi vector [pAAV2-hSyn-mCherry-miRNA-WPRE-pA; Cat. No. AI014; Shanghai Taitool Bioscience Co., Ltd. (human synapsin1; hSyn)].

The vectors were cut with restriction endonucleases in a 50-μL system containing 41 μL of double-distilled water, 5 μL of 10× CutSmart Buffer (NED; Cat. No. B7204), 2 μL of purified vector DNA (1 μg/μL), 1 μL of AgeI (10 U/μL; NED; Cat. No. R0552), and 1 μL of EcoRI (10 U/μL; NED; Cat. No. R0101). The mixture was incubated at 37°C for 3 h. Linearized vectors were harvested by agarose gel electrophoresis (Biowest Agarose; Cat. No. Q-0024796), using 120 V for 30 min. The double-enzyme-cut linearized vectors were ligated with miRNA by T4 DNA ligase (Thermo; Cat. No. EL0016) at 16°C overnight. The system contained 1 μL of linearized vector (100 ng/μL), 1 μL of miRNA (100 ng/μL), 2 μL of 10× T4 DNA ligase buffer (Thermo; Cat. No. B69), 1 μL of T4 DNA ligase, and 15 μL of DEPC water. Ten microliters of the reaction product was added to 100 μL of DH5α-competent cells (TIANGEN; Cat. No. CB101), mixed by flicking the tube wall several times, and placed on ice for 30 min. The cells were heat shocked at 42°C for 90 s and then incubated in an ice-water bath for 2 min. Subsequently, 500 μL of lysogeny broth (LB) medium was added, and the tube was placed on a shaker at 37°C for 1 h. The bacterial liquid was spread evenly on a plate containing puromycin (2 μg/mL; Beyotime; Cat. No. ST551) and then inverted in a 37°C incubator for 16 h. The bacterial solution was transferred to 10 mL of LB liquid medium containing 2 μg/mL puromycin and cultivated overnight at 37°C for plasmid extraction according to the manual of the Endotoxin-Free Plasmid Mini-Lifting Kit (TIANGEN; Cat. No. DP118-2). Briefly, bacterium-containing miRNA plasmids were harvested and ruptured by the lysate buffer and proteinase K in the kit. After adding the neutralization buffer, the protein precipitated and could be separated by centrifugation at 12,000 rpm × 15 min (Thermo; Sorvall ST1 plus). The supernatant was collected into the adsorption column, followed by centrifugation at 12,000 rpm × 1 min. The liquid under the column was discarded, and the column was washed by the eluent. After the sample dried, the plasmid sample was dissolved in 95 μL of DEPC water.

Next, the plasmids containing miRNA were triple-transfected along with pHelper1 and pHelper2 (both helper plasmids for viral packaging purchased from Shanghai Taitool Bioscience Co., Ltd.; Cat. No. Helper 1.0 and Helper 2.0) into HEK-293 cells to package AAV2/5-gfaABC1D-mCherry-miRNA-WPRE-pA and AAV2/5-hsyn-mCherry-miRNA-WPRE-pA. The scramble AAV contained a negative control sequence of miRNA. In detail, 20 μg of miRNA plasmids, 15 μg of pHelper1, and 10 μg of pHelper2 were mixed and co-transferred into HEK293 cells (to a confluence of 70% in 100-mm dishes) using 20 μL of lipofectamine 2000. The cells were incubated at 37°C for 72 h, after which the culture medium was collected and filtered using a 0.45-μm filter. Next, the medium was centrifuged at 25,000 rpm × 2 h at 4°C (Beckman; XE-90). The supernatant was discarded and the pellet containing the viral particles was collected and dissolved in 5% glycerin and stored at −80°C. The AAV vectors were quantified by qPCR. Primers were designed according to the specific sequence of woodchuck hepatitis virus posttranscriptional regulatory element (WPRE): forward 5′-CCTTTCCGGGACTTTCGCTT-3′; reverse 5′-GCAGAATCCAGGTGGCAACA-3′. Thermo QuantStudio 5 Real-Time PCR system models were used. The program was as follows: Segment 1: (1×) Step 1: 95°C for 15s; Segment 2: (40×) Step 1: 95°C for 5 s, Step 2: 60°C for 30 s data collection and real-time analysis enabled; Segment 3: (1×) Step 1: 95°C for 60 s, Step 2: 60°C for 60 s, Step 3: 60–95°C for 30 s, +0.5°C/step. The copy number of the *WPRE* gene was calculated using the absolute quantitative method. Design and Analysis Software (version 2.4.3; QuantStudio 6/7 Pro) was used for quantification. The titer of viral particles was expressed as copy number of virus genome (V.G) per milliliter.

C57BL/6 male WT or *Oct3*$^{-/-}$ mice (∼10 wk old, $n=5$ mice per group) received bilateral supra-nigral and striatal stereotactic injections of AAV capsids (2×10^7 V.G/mL, 600 nL). Avertin was used for anesthesia (300 mg/kg i.p.). The injection was performed with a Hamilton syringe and a 33-ga needle (Hamilton) at a rate of 0.8 mm/min (substantia nigra, relative to bregma: 3.1 mm caudal, ±1.3 mm lateral, and 4.2 mm ventral; striatum, relative to bregma: −0.5 mm caudal, ±2.2 mm lateral, and 2.5 mm ventral). After the injection, the needle was maintained at the injection site for 5 min before removal. Triple antibiotic and lidocaine topical ointments were applied, and the mice were kept in a 37°C incubator for 30 min to recover. It took 4 wk

for the AAVs to take effect and to prepare for the next treatments on mice (PBS or paraquat). The process of AAV injection is summarized in Figure S1B.

Mitochondrial Division Inhibitor-1 Preparations and Animal Treatments

Mitochondrial division inhibitor-1 [mdivi-1; 3-(2,4-dichloro-5-methoxyphenyl)-2-sulfanyl-4(3H)-quinazolinone; MCE; Cat. No. HY-15886] was purchased from the MCE company. Mdivi-1 is an inhibitor of DRP1-GTPase that can pass through the blood–brain barrier and inhibit DRP1 nonselectively based on *in vitro* and mouse studies.[37,38] Mdivi-1 was dissolved in dimethyl sulfoxide (DMSO; Sigma-Aldrich; Cat. No. D8418) of a 100 mg/mL stock solution. For the i.p. injection, mdivi-1 was diluted in sterile saline (1:100, vol/vol) and gently sonicated (model S3000; Sonicator; with tapered microtip; Misonix, Inc.) at a power level of 0.5–1 for 30 s before injection. The mice treated with mdivi-1 were used as a control in the present study (inhibiting DRP1-GTPase in both neuron and astrocyte). Another cohort of mice, rather than those treated by AAVs, received mdivi-1 i.p. injections (20 mg/kg, twice a day, $n = 5$ mice per group), starting on the day of the first PQ^{2+} injection and continuing until 7 d after the PQ^{2+}-CT (Figure S1B,C).

Analysis of Locomotor Activity

Baseline behavior tests (1) started at 4 wk after AAVs injection. Another series of behavior tests (2) started after the 1-wk washout period following PQ^{2+}-CT or PBS. Difference values ("2" minus "1") were calculated for statistical analysis; $n = 10$ mice for each group. The time points of the behavior tests are summarized in Figure S1B. Between the trials, apparatuses were cleaned with 70% (vol/vol) ethanol and dried with a paper tower to avoid interference due to odor.

Rotarod

The TSE Rotarod System was used to perform rotarod tests. The apparatus was accelerated from 0 to 40 rpm over 5 min and maintained at a constant speed for an additional 1 min. The latency to fall (the time duration from the start of tests to when the mouse fell from the apparatus) was then recorded as an index of locomotor activity. Mice were trained for three consecutive days before the tests by putting the mice on the rotarod at a speed of 10 rpm for 3 min to teach them moving on the rotarod.

Gait Analysis

The Noldus catwalk system (catwalk XT) was used for the gait tests. The camera's visual field was defined as 20×10 cm, including at least five paw prints from each mouse. Mice were put at one side of the track, and an eligible run required a mouse going through the visual field with a uniform speed without any disturbance. A mouse had to achieve three eligible runs before the next mouse started its test. Before the formal tests, mice underwent a process of training for 3 d, during which the mice were put on one side of the track and let go through the track without disturbance, three times per day. Data were expressed as different values of stride length, duration, stand, and swing speed before and after drug treatment. Stride length was defined as the length of step taken by the limb in one continuous step; duration, the time required for the mice to travel from one end of the track to the other; stand, the time duration when the mouse's limb touches the ground; and swing speed, the movement speed of the limb when it was raised in the air.

Constructions of N_2a Cells with Stable Expression of DAT

N_2a cells with stable expression of DAT (N_2a-DAT) were built by transfection of lentivirus. The process of constructing lentivirus tools was similar to the process of constructing AAV tools. Briefly, full-length cDNA of *Dat* (BioeGene Co. Ltd.; Cat. No. BIOE-PL-4) was cloned into linearized vector (Genomeditech Co. Ltd.; Cat. No. PGMLV-4931), named pLVX-DAT. The vectors were cut with restriction endonucleases, including AgeI (10 U/μL; NED; Cat. No. R0552) and EcoRI (10 U/μL; NED; Cat. No. R0101) to be linearized, which were then ligated with *Dat-cDNA* by T4 DNA ligase. The plasmids were amplificated in bacterial liquid and extracted using the Endotoxin-Free Plasmid Mini-Lifting Kit.

HEK293T cells were then co-transfected with the pLVX-DAT vector together with packaging plasmids (psPAX2 and pMD2G). The cells were cultured in 6-well plates to a confluence of 50% before transfection. The process was similar to the process of constructing AAV tools. Briefly, lipofectamine 2000 was used in the co-transfection. Seventy-two hours after transfection, viral particles were isolated from the culture medium by centrifugation. Pellets were dissolved in 5% glycerin and stored at −80°C. The lentiviral particles were quantified by qPCR, during which two pairs of primers were used. Primer 1: forward 5′-CCTTTCCGGGACTTTCGCTT-3′; reverse 5′-GCAGAATCCAGGTGGCAACA-3′, to amplify viral gene (gene A); Primer 2: forward 5′-CCTGGTACATGCCACTGATG-3′; reverse 5′-AGTGTAGAGGGCAAGCCAGA-3′, to amplify HEK293 cellular gene (gene B). The titer of lentivirus was expressed as transduction units (TUs) per milliliter. *TU* was calculated by $N \times C/V$, where N is the number of cells in corresponding wells of a 24-well plate at the time of infection; C is the number of viral particles in each cell, which was calculated by $(\text{copy number of gene A}/\text{copy number of gene B}) \times 2$; and V, is the volume of the viral particles used in the corresponding wells.

N_2a cells were seeded into 6-well plates (5×10^5 cells per well). The next day, the cells were incubated with the lentivirus containing the *Dat* plasmid carrying puromycin resistance gene [multiplicity of infection (MOI) = 5]. After incubation for 72 h, the medium containing the lentivirus was replaced by a culture medium containing 2-μg/mL puromycin so that cells with a stable expression of DAT survived and were selected for further experiment.

Isolation and Culture of Primary Astrocytes

Primary astrocyte cultures were harvested from Day 1 postnatal C57BL/6 mice (purchased from JSJ Laboratory Animal Technology Co., Ltd.), as previously described.[39] Briefly, brain tissues from postnatal mice were isolated intact and meninges were peeled off. The brain tissues were transferred into 15-mL centrifuge tubes with 3 mL of DMEM and homogenized by soft pipetting with Pasteur straws and 1-mL tips. The supernatant containing the cell suspension was collected and replaced by new DMEM until the visible pellet disappeared. The collected cell suspension was filtered using a 70-μm strainer and centrifuged at 1,000 rpm for 10 min at 4°C. The pellet was collected, resuspended, and plated in T-75 flasks. The cells were cultured in DMEM, 10% vol/vol FBS, and 1% P/S. Once the cells reached confluence, microglia was cleaned away using a CD11b positive selection kit (Stemcell; Cat. No. 18770) according to the manufacturer's instructions. The incubator environment was maintained at 37°C and 5% CO_2.

PQ^{2+} Treatments and Endogenous DRP1 Examination

For primary astrocyte and DAT-expressing N_2a cell treatment, PQ^{2+} was diluted in culture medium to a working concentration of 200 or 400 μM. Before being added to cells, sodium dithionite

(SDT; Sinopharm; Cat. No. 80116718) was mixed with PQ^{2+} to a final working concentration of 0.5 mM to reduce PQ^{2+} to PQ^{+}. Especially to inhibit OCT3 function in DAT-expressing N_2a cells, Decynium 22 (D22; R&D; Cat. No. 977-96-8) was mixed with PQ^{2+} and SDT to a final concentration of 5 μM, to block the transportation activity of OCT3. After incubation for 20 min, the cells were washed with PBS three times and changed to a normal culture medium for 48 h. Cells were lysed using RIPA buffer (Beyotime Cat. No. P0013B). One hundred microliters of buffer was added onto $\sim 5 \times 10^6$ cells. The mixture of buffer and cells was allowed to react on ice for 30 min. Then the lysate was scraped off and collected for Western blotting to detect changes in DRP1 levels.

DRP1 Knockdown by Small Interfering RNA

GL261 cells were plated into 24-well plates with a confluence of 50%. Drp1 small interfering RNA (siRNA) (5′-GGCAAUU-GAGCUAGCGUAUAU-3′, Shanghai Bioegene Co., Ltd.; Cat. No. BIOE-SI-KD-1) and Lipofectamine 2000 (Invitrogen; Cat. No. 2209775) were diluted with DMEM and mixed in equal volumes according to the manufacturer's instruction. After incubation for 20 min at room temperature, the mixture was added into 24-well plates (25 pmol siRNA, 1.25 μL Lipofectamine 2000 in 500 μL of DMEM per well). After 6 h, the medium was replaced with fresh medium, and the cells were cultured for 48 h for further treatment.

PQ^{2+}/PQ^{+} Uptake Assay

The functions of different PQ^{2+}/PQ^{+} transporters were tested in GL261 cells, both in normal cells and Drp1-siRNA transfected cells. The cells were treated with PQ^{2+} in diverse concentrations varying from 200, 400, 600, to 800 μM, with or without 0.5 mM SDT. The experiments included triplicated trials each time, and average values were calculated for statistics. Six independent experiments were conducted in total. A total of 10^5 cells per well were plated into a 24-well plate. To block OCT3, D22 was added with PQ^{2+} and SDT to GL261 cells in a final concentration of 5 μM. To block ASCT2, benzylserine (Benser; Sigma; Cat. No. B7283) was added together with PQ^{2+} and SDT or PQ^{2+}/SDT/D22 in a final concentration of 10 μM. After incubation with PQ^{2+}, SDT, and different inhibitors for 20 min, the cells were washed three times with PBS and lysed. Then the intracellular PQ^{2+} concentration was detected by high-performance liquid chromatography (HPLC).

HPLC

A four-channel CoulArray (ESA, Inc.) equipped with a highly sensitive amperometric microbore cell (model 5041; ESA, Inc.) was used to analyze the content of DA and PQ^{2+} in the dialysates after *in vivo* microdialysis. The cell potential was set at 220 mV. In brief, 20-μL samples were manually injected into a sample injector (with a 20-μL sample loop) and eluted on a narrow-bore (ID: 2 mm) reverse-phase C18 column (MD-150; ESA, Inc.) using MD-TM (ESA, Inc.) mobile phase. DA and PQ^{2+} were detected using an ultraviolet detector (model 526; ESA, Inc.). Samples were manually injected and separated by a narrow-bore column (ID: 2.1 mm; Altima HP C18; Alltech Associates, Inc.) using mobile phases consisting of 80.5% 50 mM monopotassium phosphate (Sigma; PRH1330) and 9.5% acetonitrile (Sigma; Cat. No. 34851), pH 3.2. The flow rate was set at 0.2 mL/min for all measurements using a solvent delivery pump (model 585; ESA, Inc.).

Mdivi-1 Treatment in GL261 Cells

For cell treatment, the mdivi-1 stock solution was diluted in a culture medium to 10 μM. To inhibit DRP1 levels in GL261 cells, the culture medium containing 10 μM of mdivi-1 was added and incubated for 24 h before the PQ^{+} treatment.

Isolation and Culture of Primary Neurons

Primary neurons were harvested as previously documented.[40] Three-centimeter culture plates were coated with 1 mg/mL poly L-lysine (Sigma; Cat. No. P2636) for 24 h in 37°C incubators. The embryos were removed from pregnant female C57BL/6 mice (16.5 d; purchased from JSJ Laboratory Animal Technology Co., Ltd.) and placed into ice-cold Hank's balanced salt solution (HBSS; R&D; Cat. No. B31250). The brain tissues were taken out and meninges were peeled off, followed by digesting in 5 mL of 0.25% trypsin (Gibco; Cat. No. 25200056) at 37°C for 15 min, gently shaking at 180 rpm. Then 10 mL of DMEM was added to stop the digestion. The digested tissues were collected in new tubes and disassociated by soft pipetting with 3-mL Pasteur straws until the visible pellet disappeared. The supernatant containing cell suspension was collected and filtered using a 70-μm strainer. After centrifugation at 1,000 rpm for 10 min at 4°C, The pellet was collected and resuspended in neurobasal medium (Gibco; Cat. No. 21103049) containing b27 supplement (Gibco; Cat. No. 17504044, added at a 1:50 ratio). Primary neurons were plated into coated 3-cm dishes at 5×10^5 per dish, culturing at 37°C in 5% CO_2.

Western Blotting Analysis

The protein concentrations of samples were evaluated according to the manual of the Pierce bicinchoninic acid assay for protein quantity kit (Thermo; Cat. No. 23225). Briefly, the protein standards were diluted into concentrations of 25, 50, 100, 250, 500, 1,000, 1,500 and 2,000 μg/mL. Reagents A and B in the kit were mixed at 50:1. Two hundred microliters of the AB mixture and 25 μL of the sample or protein standards were mixed and added into a well of 96-well culture plates, followed by incubation at 37°C for 30 min. The absorbance value was detected at 562 nm using an H1 Hybrid reader (Bio-Rad). Protein (30 μg) was added to lanes in 10% sodium dodecyl sulfate–polyacrylamide gel electrophoresis (SDS-PAGE) gel (Beyotime; Cat. No. P0690). After electrophoresis, the protein was transferred onto 0.22-μm polyvinylidene difluoride (PVDF) membranes with a constant current of 250 mA for 90 min. The membranes were blocked with 5% wt/vol bovine serum albumin (BSA) for 1 h and incubated in primary antibodies (1:1,000 vol/vol) of DRP1 (Cell Signaling Technology; Cat. No. 8570), ASCT2 (Cell Signaling Technology; Cat. No. 8057), SLC1A4 (Cell Signaling Technology; Cat. No. 8442), 4F2hc (Cell Signaling Technology; Cat. No. 47213), β-actin (Cell Signaling Pathway; Cat. No. 13E5), and OCT3 (Affinity; Cat. No. AF5358) separately at 4°C overnight. The next day, after extensive washing, membranes were incubated with horseradish peroxidase (HRP)-conjugated secondary antibodies (Yeasen; Cat. No. 33101ES60) (1:5,000, vol/vol) for 1 h. The blots were visualized using HRP substrate peroxide solution (Millipore; Cat. No. WBKLS0500). The relative optical density (ROD) of the protein of interest and β-actin were analyzed using ImageJ software.

In Vivo Microdialysis for Detections of DA Release and Cerebral Extracellular PQ^{2+}

In vivo microdialysis was processed as previously reported.[21] Briefly, the mice were anesthetized by 2.5% (wt/vol) avertin at 300 mg/kg. Stereotactic implantation of the guide cannula

(CMA; Harvard Bioscience, Inc.) into the striatum was performed using the following striatal coordinates relative to bregma: anterior–posterior+0.5 mm, lateral 2.0 mm, and dorsal–ventral 1.5 mm (from the surface of the brain). The next day, a microdialysis probe (CMA8 with 2 mm membrane length; CMA; Harvard Bioscience, Inc.) was inserted into the guide cannula and connected to a low-torque dual channel swivel (Instech Laboratories, Inc.). The channel was connected by the PEEK tube (Cat. No. 8409501) to a syringe pump perfusing artificial cerebrospinal fluid (aCSF). aCSF was purchased from Phygene company (Cat. No. PH1851). After a 2-h equilibration period, dialysates were collected for all DA release studies and detections for extracellular PQ^{2+} in the brains of the mice. To observe DA release, dialysates were collected every 15 min. One baseline fraction was collected, after which the perfusate was switched to aCSF containing 100 mM potassium chloride (KCl; with an equimolar reduction in sodium chloride to maintain osmolality) for 15 min to deliver a total of 240 nmol KCl, followed by a return to normal aCSF for 45 min. DA was measured in each sample simultaneously. To measure extracellular PQ^{2+}, the probe was continuously perfused with normal aCSF for 30 min and dialysates were collected. Probe efficiency was 8%, and flow rate, 2 μL/min. DA and PQ^{2+} in the dialysates were measured by HPLC, as previously described.

Immunohistochemistry

The mice were anesthetized using 2.5% (wt/vol) avertin at 300 mg/kg (Sigma-Aldrich; Cat. No. T48402) and perfused with an ice-cold saline solution followed by 4% wt/vol PFA (Sangon Biotech; Cat. No. A500684). Brain tissues were post-fixed with 4% PFA for 12 h and then gradually dehydrated in 10%, 20%, and 30% wt/vol sucrose (dissolved in 0.1 M PBS, pH 7.2) for 72 h in total. After being embedded in optimal cutting temperature (O.C.T.) gel (SAKURA; Cat. No. 4583) and quick-frozen at −80°C, the brains were frontally sectioned using a freezing microtome, and 30-μm sections were sequentially collected in four- (substantia nigra) or eight- (striatum) section series. Endogenous peroxidase activity was inhibited by bathing twice for 15 min in 1% hydrogen peroxide/PBS (0.01 M, pH 7.4). After washing, sections were incubated for 2 h in blocking buffer [0.1% TX-100/10% normal goat serum (NGS)/0.01 M PBS, pH 7.4]. The tyrosine hydroxylase (TH) staining process was performed according to the manufacturer of the Vectastain Elite ABC HRP Kit (Vector Laboratories; Cat. No. PK6100). Briefly, brain sections were incubated at 4°C overnight with anti-TH primary antibody (1:500 in PBS containing 2% NGS; Abcam Cat. No. ab112), followed by 2 h in biotinylated secondary antibodies (Vector BA-1000, diluted at 1:200 in PBS containing 2% NGS, vol/vol). Then 3,3′-diaminobenzidine (DAB) substrate (Peroxidase; Vector Laboratories) was used for color development. The sections were then placed on glass slides and subjected to Nissl staining, as described below. An Olympus camera (DP72; Olympus) was used to take images. The quantification of TH-positive cells was achieved by stereoscopic counting, as described below. As to detections of optical density, six to eight sections per mice were analyzed, with $n = 10$ mice per group.

Nissl Staining

The brain sections on object-glass slides were incubated with Nissl staining solution (Solarbio; Cat. No. G1430) at 56°C for 1 h, then decolorized for 5 min at room temperature. Next, the sections were sequentially dehydrated by 75% and 100% ethanol and immersed into dimethylbenzene for 5 min; this procedure was repeated in triplicate. Finally, the microslides were covered with neutral gum (Solarbio; Cat. No. G8590) and cover slips. Nissl bodies in the soma of neurons were stained blue and counted stereoscopically.

Quantifications of TH-Positive and Nissl Neurons

TH-positive cells and Nissl bodies in the substantia nigra pars compacta (SNpc) were analyzed by stereoscopic counting using Stereo Investigator software (version 7; MicroBrightField) and a photomicroscope (Olympus BX53), as previously reported.[41] Briefly, an area of SNpc in the substantia nigra was selected as the counting range, in which frame size was under 400× magnification (set to be 60 × 80 mm under 40× magnification). TH-positive cells in each frame were counted manually, and the total cell numbers were calculated in the ipsilateral SNpc. Striatal TH fiber optical density was scanned in a high-resolution scanner and measured using ImageJ software.

Immunofluorescence Staining

The cerebral sections were incubated in 5% BSA (MP Biomedicals Cat. No. 02FC007791) for 2h. After three washes, the sections were incubated with rabbit anti-ASCT2 (1:100; Cell Signaling Technology; Cat. No. 8057), TH (1:1,000), DRP1 (1:500; Cell Signaling Technology; Cat. No. 8570), and chicken anti-GFAP (1:1,000; Abcam; Cat. No. ab4674) vol/vol primary antibodies at 4°C overnight. After three washes, the sections were incubated with goat anti-rabbit Alexflour488 (Yeasen; Cat. No. 33106ES60) and goat anti-chicken Alexflour647 (Abcam; Cat. No. ab150157) secondary antibodies at room temperature for 2 h (1:1,000 vol/vol). The sections were observed under a confocal microscope (Olympus FV-10). Six to eight sections were analyzed per mouse. Ex/Em spectra were as follows: Alexflour405, 401 nm/421 nm; Alexflour488, 499 nm/519 nm; Alexflour594, 591 nm/618 nm and Alexflour647, 652 nm/668 nm.

Statistical Analysis

Data were analyzed and graphed with GraphPad Prism 8 software (version 8.0.2). All the data from the mice are represented as mean ± standard deviation (SD), and data from cells are represented as mean ± standard error of the mean (SEM). Different treatment groups were evaluated using an unpaired *t* test, a one-way analysis of variance (ANOVA), or a two-way ANOVA. Post hoc tests were done for multiple pairwise comparisons after one- and two-way ANOVAs to determine differences among individual groups. Post hoc tests were corrected by the Bonferroni method. The null hypothesis was rejected when the *p*-value was <0.05. $^{*}/^{\#}$, $p < 0.05$; $^{**}/^{\#\#}$, $p < 0.01$; $^{***}/^{\#\#\#}$, $p < 0.001$.

Results

The Cerebral Expression Level of OCT3 in Mice of Different Ages with or without PQ^{2+}–CT

It remained unknown whether the levels of OCT3 could change with the progression of aging or PQ^{2+} treatment. Thus, OCT3 levels in the brains of different-aged mice with or without PQ^{2+} chronic treatment (PQ^{2+}-CT) were analyzed. Brain OCT3 levels in the older mice were significantly lower than in younger ones. Furthermore, after stratifying mice based on their ages, the brain OCT3 levels were lower in the mice that received PQ^{2+}-CT than in those that received PBS (Figure 1A,B). To assess the capacity of the brain to remove the extracellular PQ^{2+}, another loading dose of PQ^{2+} (10 mg/kg; LT) was injected after a 1-wk washout period following the PQ^{2+}-CT or PBS treatment. *In vivo* microdialysis was performed to detect the extracellular PQ^{2+} residues.

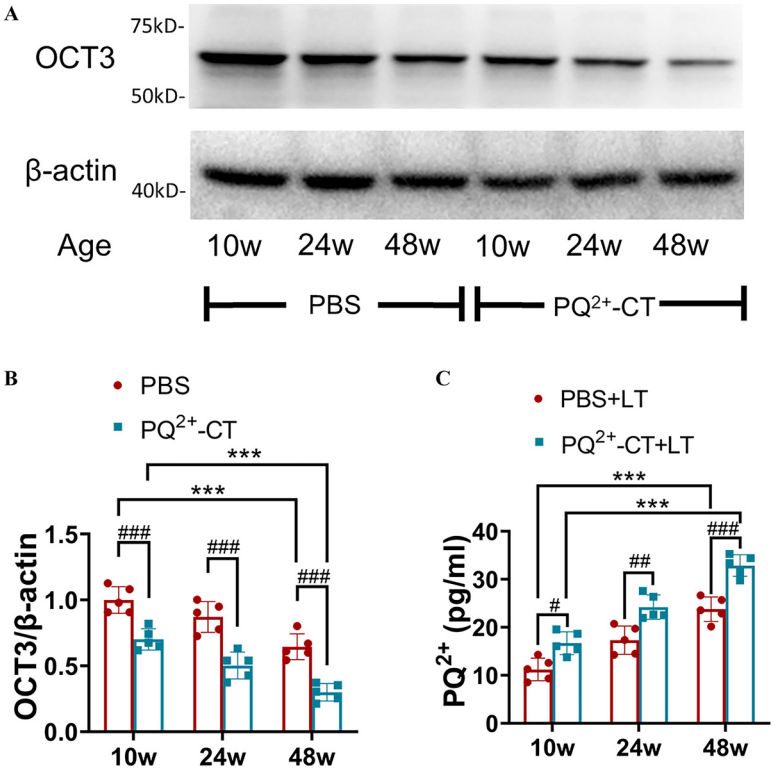

Figure 1. Detection of OCT3 levels and extracellular residue of loading PQ^{2+} in the brains of mice with different ages. (A) Representative images showing the levels of OCT3 in the brains of 10-, 24-, and 48-wk-old C57BL/6 mice with or without PQ^{2+} chronic treatment (PQ^{2+}-CT). (B) Quantitative analysis of OCT3/β-actin. $n = 5$ mice per group. (C) The extracellular levels of the loading dose of PQ^{2+} [PQ^{2+}-loading treatment (LT)] in the brains of mice with different ages. $n = 5$ mice per group. Data are shown as mean ± SD. Two-way ANOVAs were followed by the Bonferroni multiple comparisons test. $^{\#}$, $p < 0.05$; $^{\#\#}$, $p < 0.01$; $^{***/\#\#\#}$, $p < 0.001$. The numeric data are shown in Excel Table S1. In two-way ANOVAs, "*" was used to present the statistical difference between groups both treated by PBS or PQ^{2+}, and "#" was used to present the statistical difference between the PBS- and the PQ^{2+}-treated groups. Note: ANOVA, analysis of variance; CT, chronic treatment; OCT3, organic cation transporter-3; PQ, paraquat; SD, standard deviation.

The results suggested that consistent with the lower brain OCT3 expression levels, extracellular residues of the loading dose PQ^{2+} was higher in the older mice and in mice that received PQ^{2+}-CT than in the younger ones and in PBS-treated mice (Figure 1C).

The Location and Expression of DRP1 after PQ^{2+}–CT in WT or $Oct3^{-/-}$ Mice

To date, the relationship between PQ^{2+} and DRP1, especially astrocyte DRP1, remains undetermined. We detected the DRP1 levels in the substantia nigra of WT and *Oct3*$^{-/-}$ mice with or without PQ^{2+}-CT. Our results showed DRP1 levels were higher in mice that received PQ^{2+}-CT than in those treated with PBS, both in neurons and astrocytes (Figure 2A–C). Besides animal experiments, we also detected DRP1 changes in cultured neurons and primary astrocytes. To facilitate the entry of PQ^{2+} into cells, we treated the cells with PQ^{2+} and SDT. This reducing agent was used to donate an electron and hence convert PQ^{2+} to PQ^{+}. In N_2a-DAT cells without Decynium 22 (D22; a blocker of OCT3) treatment, 400 μM PQ^{+} (reduced from PQ^{2+} by SDT) treatment induced a higher level of DRP1 (Figure 2D,F). In primary astrocytes from WT mice, PQ^{+} treatment induced a higher level of DRP1 in a dose-dependent manner (Figure 2E,H). Although OCT3 has a limited expression on neurons, D22 was used to inhibit the potential transporting activity of OCT3. Compared with the N_2a-DAT cells treated with PBS, DRP1 levels were not influenced by D22 (Figure 2D,G). In primary astrocytes from *Oct3*$^{-/-}$ mice, PQ^{+} still induced a dose-dependent DRP1 upregulation (Figure 2E,I).

The Effects of Selective Neural and Astrocyte DRP1 Knockdown on PQ^{2+}-Induced Neurotoxicity in WT and $Oct3^{-/-}$ Mice

Higher DRP1 protein level in both neurons and astrocytes after PQ^{2+}/PQ^{+} treatment suggested that DRP1 could be involved in the toxic effects of PQ^{2+}/PQ^{+}. The present study tested the impact of DRP1 inhibition in a PQ^{2+}-induced PD model with or without *Oct3* deficiency. Mdivi-1, an inhibitor of DRP1-GTPase that can pass through the blood–brain barrier and inhibit DRP1 in both neurons and astrocytes[42], was used as a control. Selective DRP1 knockdown was achieved by stereotactic injections of AAV, which had no effect on the death of TH-positive cells compared with PBS treatment (Figure S2A,B) but had considerable efficiency of DRP1 knockdown (Figure S3A,B) and selectivity of neurons or astrocytes with neural (hsyn) or astrocyte (gfaABC1D) promotor (Figure S3C). There were 10 mice/group and all of them went through the whole process of experiments. Their body weight was measured before the behavior tests (1 and 2) and during the process of PBS/PQ^{2+}-CT (Figure S1B). No statistical difference was observed in the comparations among mice in different groups or at different time points (Figure S4A,B). Results revealed that the number of TH neurons, density of striatal TH terminals, and dopamine release were not influenced by selective DRP1 knockdown in either WT mice or *Oct3*$^{-/-}$ mice without PQ^{2+}-CT (Figures 3A–H and 4A–H). After PQ^{2+}-CT, the number of TH-positive neurons was lower (Figure 3A,C), but the striatal TH terminals or dopamine release was spared in WT mice (Figure 3D,F–H). The lower number of nigral TH-positive cells was ameliorated in the mice that received neural DRP1 knockdown and mdivi-1 rather than DRP1

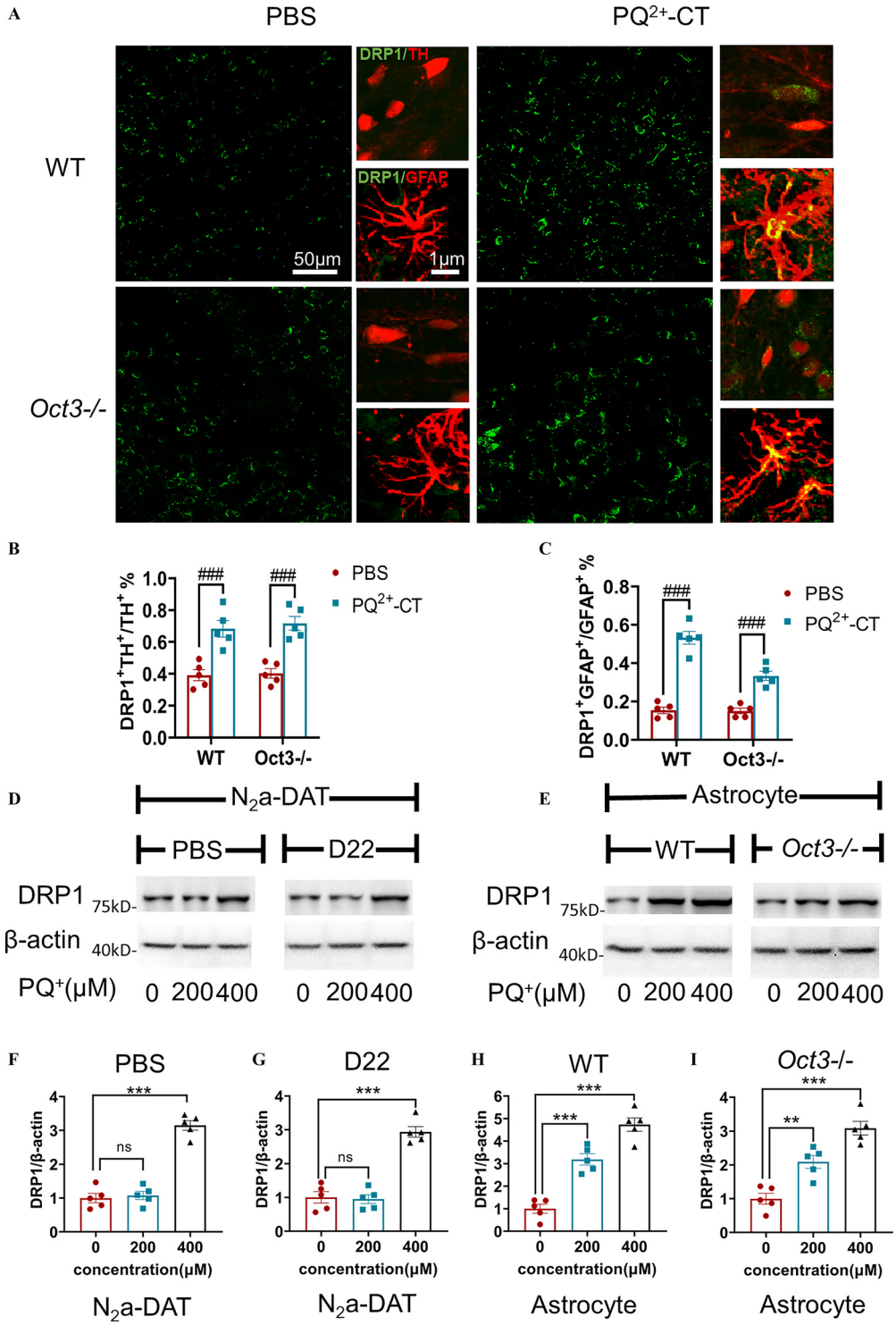

Figure 2. DRP1 level in the brains of mice and in cultured cells exposed to PQ^{2+} or PQ^{+}. (A) Representative immunofluorescent staining of DRP1 in the substantia nigra of WT and *Oct3*$^{-/-}$ mice. The expression of DRP1 after PQ^{2+}-CT and the colocalization of DRP1 with TH and GFAP-positive cells is shown. (B) Cells positive for TH^{+} and $TH^{+}DRP1^{+}$ immunofluorescence were counted, and the proportion of $TH^{+}DRP1^{+}/TH^{+}$ was quantified. (C) Cells positive for $GFAP^{+}$ and $GFAP^{+}DRP1^{+}$ immunofluorescence were counted, and the proportion of $GFAP^{+}DRP1^{+}/GFAP^{+}$ was quantified. $n = 5$ mice per group. Six to eight sections were analyzed per mouse. The average value per mouse was used for statistics. Two-way ANOVAs were followed by the Bonferroni multiple comparisons test. Data are shown as mean ± SEM. (D,E) DRP1 protein levels in N_2a-DAT neuronal cells (with or without D22 added to culture media to inhibit the potential activity of OCT3) and primary astrocytes (from WT or *Oct3*$^{-/-}$ mice) were detected by Western blot following reduction PQ^{2+} to PQ^{+} by SDT and addition at concentrations of 0, 200, or 400 μM. (F–I) Quantitative analysis of DRP1/β-actin. The 0-μM group was normalized to 1. $n = 5$ per group. One-way ANOVA was followed by the Bonferroni multiple comparisons test. Data are shown as mean ± SEM. *, $p < 0.05$; **, $p < 0.01$ $^{***/\#\#\#}$, $p < 0.001$; ns, no significance. The numeric data are shown in Excel Table S2. In two-way ANOVAs, "#" was used to present the statistical difference between the PBS- and the PQ^{2+}-treated groups. Note: ANOVA, analysis of variance; CT, chronic treatment; D22, Decynium 22; DRP1, dynamic related protein-1; GFAP, glial fibrillary acidic protein; N_2a-DAT, N_2a neural cells with stable expression of dopamine transporter; OCT3, organic cation transporter-3; PBS, phosphate-buffered saline; PQ, paraquat; SDT, sodium dithionite; SEM, standard error of the mean; TH, tyrosine hydroxylase; WT, wild-type.

knockdown in astrocytes (Figure 3A–C,E). PQ^{2+}-CT had no influence on the behavior performance of WT mice, neither did DRP1 inhibition in neurons, astrocytes, or both (Figure 3I,J; Figure S4C,E). In the *Oct3*$^{-/-}$ mice, comparatively fewer DA neurons were observed after treatment with PQ^{2+}, with significantly less immunoreactivity of striatal TH. Similar to the WT mice, the PQ^{2+}-induced neurotoxicity was relieved by selective neural DRP1 knockdown and mdivi-1 treatment; however, selective astrocyte DRP1 knockdown also attenuated the PQ^{2+}-induced pathological changes in the nigrostriatal system that had no significant difference in neural DRP1 knockdown (Figure 4A–E). To evaluate the DA synaptic function, we used *in vivo* microdialysis to assess depolarization-induced DA overflow in the striatum of freely moving *Oct3*$^{-/-}$ mice. After PQ treatment, *Oct3*$^{-/-}$ mice exhibited significantly less DA overflow; a restoration of evoked DA overflow was achieved by selective astrocyte DRP1 knockdown and was more effective than neural DRP1 knockdown (Figure 4F–H). The locomotor performance in *Oct3*$^{-/-}$ mice were also improved by astrocyte DRP1 knockdown. (Figure 4I,J; Figure S4D,F).

The Capacity of the Nigrostriatal System to Clear Extracellular PQ^{2+}/PQ^{+} after Astrocyte DRP1 Inhibition

As reported above, selective astrocyte DRP1 knockdown ameliorated the PQ^{2+}-induced neurodegeneration in the mice with *Oct3* deficiency, and the mechanisms remained undemonstrated. We hypothesized that astrocyte DRP1 knockdown might enhance the PQ^{+} clearance in astrocytes and that this would not occur in WT mice. To elucidate this hypothesis, a loading dose of PQ^{2+} (PQ^{2+}-LT) was injected and *in vivo* microdialysis was performed to detect extracellular PQ^{2+} in the striatum in both WT and *Oct3*$^{-/-}$ mice after neural or astrocyte DRP1 knockdown. *Oct3*$^{-/-}$ mice had significantly higher levels of extracellular PQ^{2+} than WT mice, and this difference was much less pronounced after selective astrocyte DRP1 knockdown in *Oct3*$^{-/-}$ mice. By contrast, no differences in extracellular PQ^{2+} were observed between WT mice exposed to either empty AAV control, neuronal DRP knockdown by AAV, astrocyte DRP1 knockdown by AAV, or non-selective DRP1 knockdown using mdivi-1. (Figure 5A,B). To support the hypothesis that DRP1 knockdown might contribute to astrocytic PQ^{2+} clearance in *Oct3*$^{-/-}$ mice, *in vitro* transport assays were conducted using a cultured astrocyte cell line. Regardless of whether Drp1 siRNA was added, astrocytes had very limited capacity to uptake PQ^{2+} (Figure 5C). After PQ^{2+} was converted to PQ^{+} by SDT, the intracellular content of PQ^{+} was dramatically higher, suggesting considerable PQ^{+} uptake by cultured astrocytes. Accordingly, PQ^{+} transport could be significantly inhibited by D22, indicating the critical role of OCT3 in the transport of extracellular PQ^{+} to astrocyte. Furthermore, Drp1 siRNA partially reestablished the PQ^{+} transport originally blocked by D22 (Figure 5D).

Expressions of Astrocytic PQ^{+} Transporters after DRP1 Knockdown

To further clarify the mechanism of the greater uptake of PQ^{+} in astrocytes after DRP1 knockdown, the differences in the expression levels of three major monovalent cation transporters, including SLC1A4, ASCT2, and 4F2hc, were examined in the cultured astrocyte cell line. The level of ASCT2 was significantly higher in cells treated with Drp1 siRNA and mdivi-1, whereas the levels of other two monovalent cation transporters did not differ between the groups (Figure 6A–H). Besides, PQ^{+} itself had a limited impact on the expression of these transporters.

In vivo immunofluorescent staining was conducted to locate the distribution of highly expressed ASCT2. Confocal scanning showed that selective astrocyte DRP1 knockdown or mdivi-1-treated *Oct3*$^{-/-}$ mice and WT mice had higher expression of ASCT2. The ASCT2 was mainly colocalized with GFAP, the marker of astrocytes (Figure 7A–E), but rarely distributed on neurons (Figure S5A–D).

The Comparation of PQ^{+} Transportation Activity between ASCT2 and OCT3

Although higher expression of ASCT2 was observed in both WT and *Oct3*$^{-/-}$ mice after astrocyte DRP1 knockdown, the greater clearance of extracellular PQ^{2+} only occurred in *Oct3*$^{-/-}$ mice. As presented above, selective astrocyte DRP1 inhibition restored the PQ^{+} transport capacity of astrocytes and relieved PQ^{2+}-induced neurodegeneration in *Oct3*$^{-/-}$ mice. This observation led us to hypothesize that OCT3 accumulated more PQ^{+} than ASCT2 could, which may be related to the transporter expression level, affinity, and maximal transport rates. To compare the affinity of the two transporters for PQ^{+}/PQ^{2+}, we performed a transport study using cultured astrocyte cell lines. The PQ^{2+} uptake by astrocytes was limited and was not affected by Drp1 siRNA or transporter blockers (Figure 8A,B). When PQ^{2+} was converted to PQ^{+} by reducing agent SDT, a higher uptake of PQ^{+} into astrocytes was observed, which was mitigated by treatment with D22 (blocker of OCT3), but not Benser (blocker of ASCT2), indicating that OCT3 might have a higher affinity for PQ^{+} than ASCT2 under physiological conditions (Figure 8C). When astrocyte DRP1 was knocked-down by siRNA (which led to higher protein expression of ASCT2 in GL261 astrocytes; Figure 6), Benser partially inhibited the PQ^{+} uptake, but had a weaker inhibitory effect than D22. Of note, in astrocytes treated by Drp1 siRNA, when OCT3 was blocked by D22, Benser further reduced the uptake of PQ (Figure 8D).

To further test the complementary role of ASCT2 in extracellular PQ^{2+} clearance *in vivo*, we used *in vivo* microdialysis after PQ^{2+}-LT and applied aCSF containing Benser to observe the role of ASCT2 in clearing extracellular PQ^{2+} in *Oct3*$^{-/-}$ mice and WT mice. Benser had a limited impact on extracellular PQ^{2+} levels in WT mice (Figure 9A). *Oct3*$^{-/-}$ mice demonstrated higher extracellular PQ^{2+}than WT mice, but treatment with selective astrocyte DRP1 knockdown or mdivi-1 resulted in lower extracellular PQ^{2+} concentrations. More importantly, Benser infusion mitigated the effect of DRP1 inhibition such that extracellular PQ^{2+} levels were significantly higher in mice treated with Astro-DRP1 KD and Mdivi-1 plus Benser than in the corresponding groups without Benser (Figure 9B).

Discussion

Epidemiological studies indicated that PD is a complex disease caused by the interaction of genetic and environmental factors.[42,43] However, only 10% of PD cases can be attributed to the disease-causing gene. There are no definite pathological mutations in most PD patients,[8] indicating that environmental factors play an important role in the pathogenesis of PD. Epidemiological and experimental studies reported that many substances have been found to increase the risk of PD including PQ^{2+}.[9,16] PQ^{2+} has a similar chemical structure of organic cation to 1-methyl-4-phenylpyridinium (MPP^{+}), the active form of 1-methyl-4-phenyl-1,2,3,6-tetrahydropyridine hydrochloride (MPTP),[44] which is a selective dopaminergic pro-neurotoxin and an acknowledged inducer of PD phenotype in animal models.[45] Both PQ^{2+} and MPP^{+} have been documented by studies in mouse and cells to disrupt mitochondrial respiratory activities, inducing the overloading of reactive oxygen species (ROS), thus accelerating the death of dopaminergic

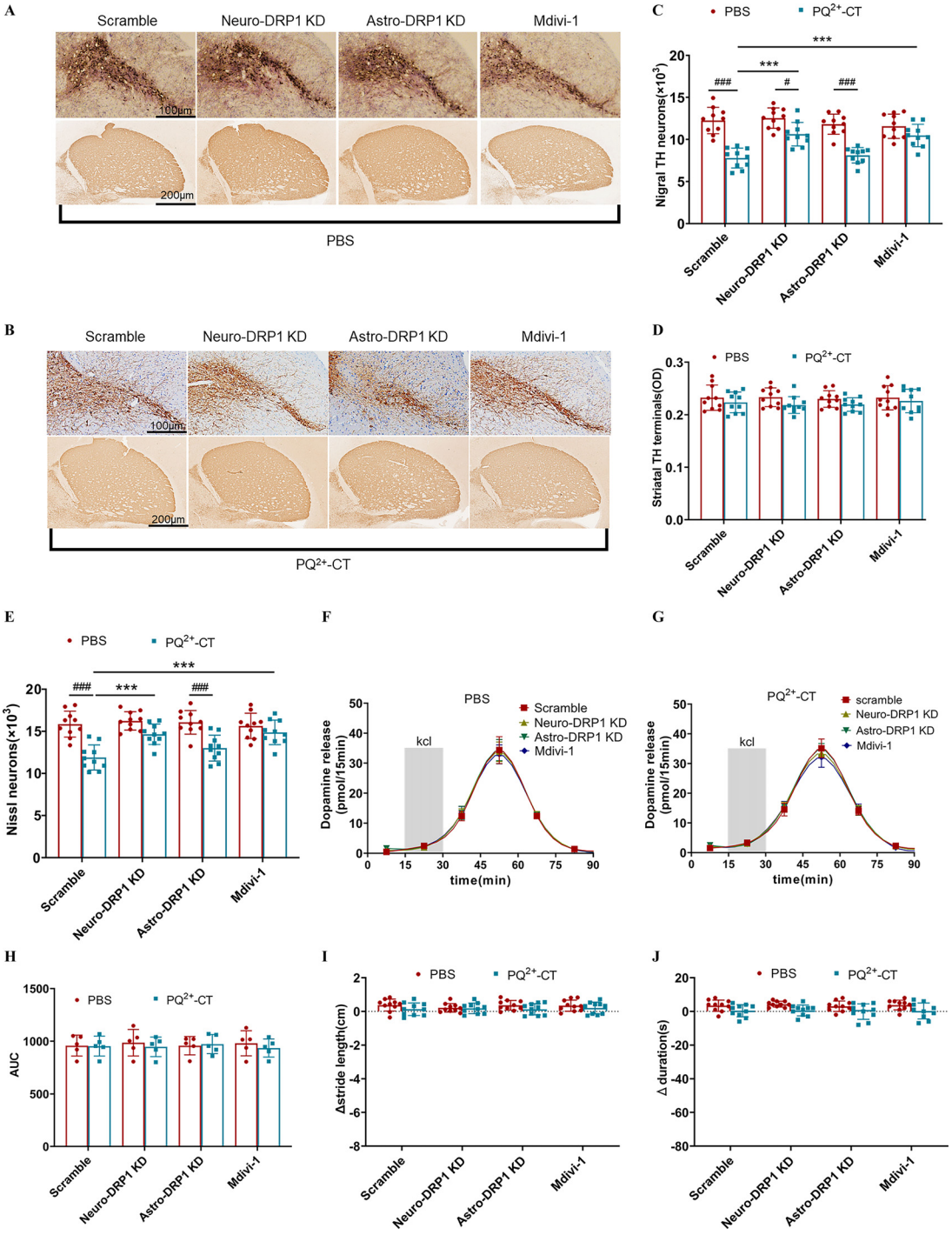

Figure 3. Measures of neurodegeneration and locomotor activity in WT mice exposed to PQ^{2+} with and without DRP1 knockdown. (A,B) IHC staining of TH-positive cells in substantial nigra and terminals in striatum from mice that received (A) PBS or (B)PQ^{2+}-CT. (C,D) Quantitative analysis of (C) TH-positive cells in SNpc and (D) striatal optical density (OD) of TH terminals. $n = 10$ mice per group. (E) Quantitative analysis of Nissl staining in SNpc. $n = 10$ mice per group. (F,G) *In vivo* microdialysis followed by HPLC tests for striatal DA release in mice that received (F) PBS or (G)PQ^{2+}-CT. To evoke depolarization-induced release of DA, 240 nmol KCl in isotonic aCSF was perfused over a 15-min period (shaded box). (H) Peak areas under curves were analyzed. $n = 5$ mice per group. (I) The differences in stride length of mice before and after PQ^{2+}-CT in mice exposed to either empty AAV control, neuronal DRP knockdown by AAV, astrocyte DRP1 knockdown by AAV, or non-selective DRP1 knockdown using mdivi-1. $n = 10$ mice per group (J) Rotarod tests of the mice in different groups. The value was measured before and after PQ^{2+}-CT, and the differences were calculated by "after" minus "before." Data are shown as mean ± SD. Two-way ANOVAs were followed by the Bonferroni multiple comparison test. *, $p < 0.05$; **, $p < 0.01$; ***/###, $p < 0.001$; ns, no significance. The numeric data are shown in Excel Table S3. In two-way ANOVAs, "*" was used to present the statistical difference between groups both treated by PQ^{2+}, and "#" was used to present the statistical difference between the PBS- and the PQ^{2+}-treated groups. Note: AAV, adeno-associated virus; aCSF, artificial cerebrospinal fluid; ANOVA, analysis of variance; Astro-DRP1 KD, DRP1 knockdown in astrocytes by AAV with gfaABC1D promoter; AUC, area under the curve; CT, chronic treatment; DA, dopamine; DRP1, dynamic related protein-1; HPLC, high-performance liquid chromatography; IHC, immunohistochemistry; KCl, potassium chloride; KD, knockdown; mdivi-1, mitochondrial division inhibitor-1; Neuro-DRP1 KD, DRP1 knockdown in neuron by AAV with hsyn promoter; OCT3;organic cation transporter-3; PBS, phosphate-buffered saline; PQ, paraquat; Scramble, empty AAV for control; SD, standard deviation; SNpc, substantia nigra pars compacta; TH, Tyrosine hydroxylase.

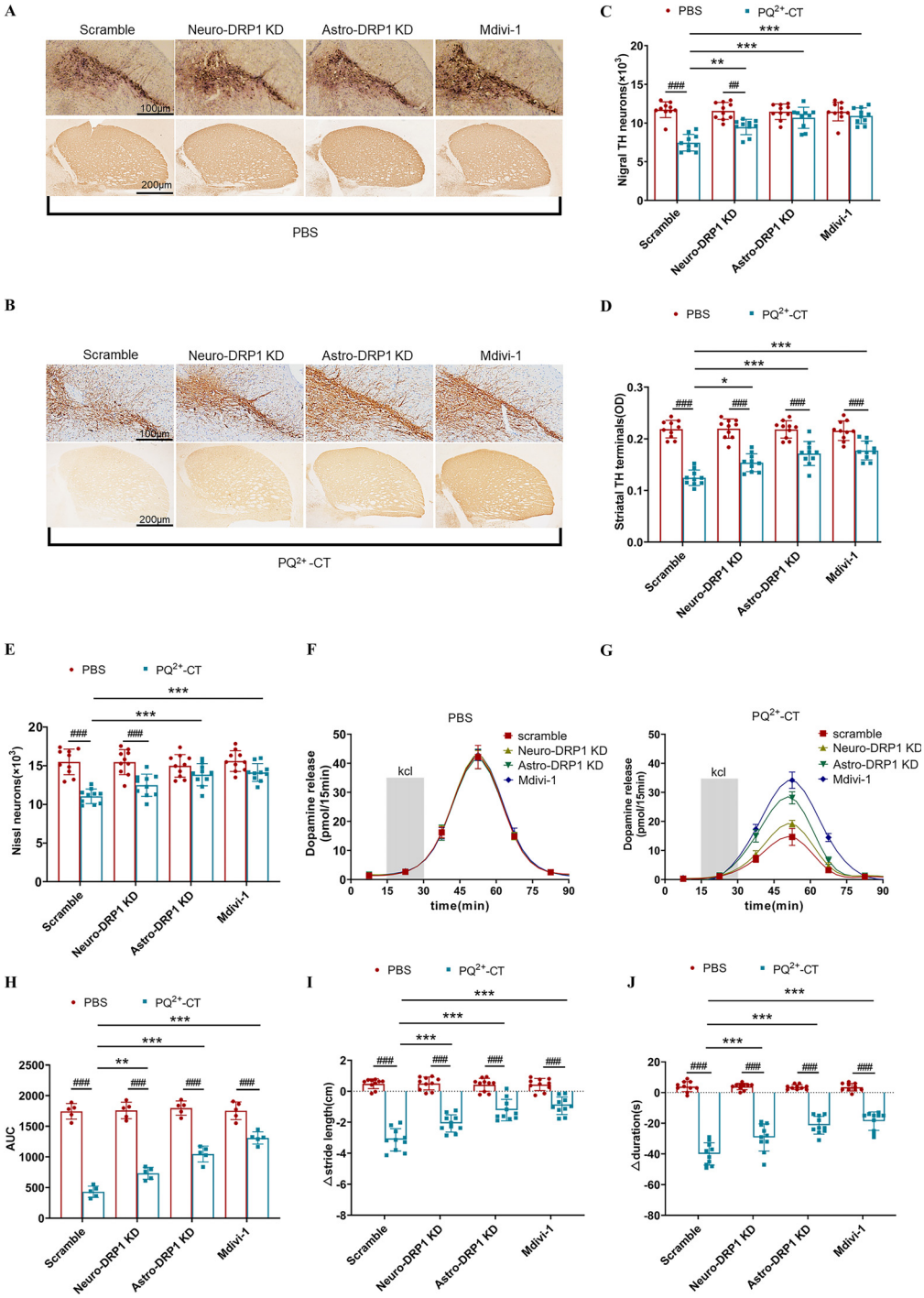

Figure 4. Measures of neurodegeneration and locomotor activity in *Oct3*$^{-/-}$ mice exposed to PQ^{2+} with and without DRP1 knockdown. (A,B) IHC staining of TH-positive cells in SNpc and striatum terminals in *Oct3*$^{-/-}$ mice that received (A) PBS and (B)PQ^{2+}-CT. (C, D) Quantitative analysis of (C) TH-positive cells in SNpc and (D) striatal optical density (OD) of TH terminals. $n = 10$ mice per group. (E) Quantitative analysis of Nissl staining in SNpc. $n = 10$ mice per group. (F,G) *In vivo* microdialysis followed by HPLC tests for striatal DA release from the brains of mice that received (F) PBS or (G)PQ^{2+}-CT. To evoke depolarization-induced release of DA, 240 nmol KCl in isotonic aCSF was delivered through the probe over a 15-min period (shaded box). (H) Peak areas under curves were analyzed. $n = 5$ mice per group. (I) The differences in stride length of mice before and after PQ^{2+}-CT in mice exposed to either empty AAV control, neuronal DRP knockdown by AAV, astrocyte DRP1 knockdown by AAV, or non-selective DRP1 knockdown using mdivi-1. $n = 10$ mice per group (J) Rotarod tests of the mice in different groups. The value was measured before and after PQ^{2+}-CT, and the differences were calculated by "after" minus "before." $n = 10$ mice per group. Data are shown as mean ± SD. Two-way ANOVAs were followed by the Bonferroni multiple comparison test. *, $p < 0.05$; **, $p < 0.01$ ***/###, $p < 0.001$. The numeric data are shown in Excel Table S4. In two-way ANOVAs, "*" was used to present the statistical difference between groups both treated by PQ^{2+}, and "#" was used to present the statistical difference between PBS-treated group and PQ^{2+} treated group. Note: AAV, adeno-associated virus; aCSF, artificial cerebrospinal fluid; ANOVA, analysis of variance; Astro-DRP1 KD, DRP1 knockdown in astrocytes by AAV with gfaABC1D promoter; AUC, area under the curve; CT, chronic treatment; DA, dopamine; DRP1, dynamic related protein-1; HPLC, high-performance liquid chromatography; IHC, immunohistochemistry; KCl, potassium chloride; KD, knockdown; Neuro-DRP1 KD, DRP1 knockdown in neuron by AAV with hsyn promoter; mdivi-1, mitochondrial division inhibitor-1; OCT3, organic cation transporter-3; PBS, phosphate-buffered saline; PQ, paraquat; Scramble, empty AAV for control; SD, standard deviation; SNpc, substantia nigra pars compacta; TH, Tyrosine hydroxylase.

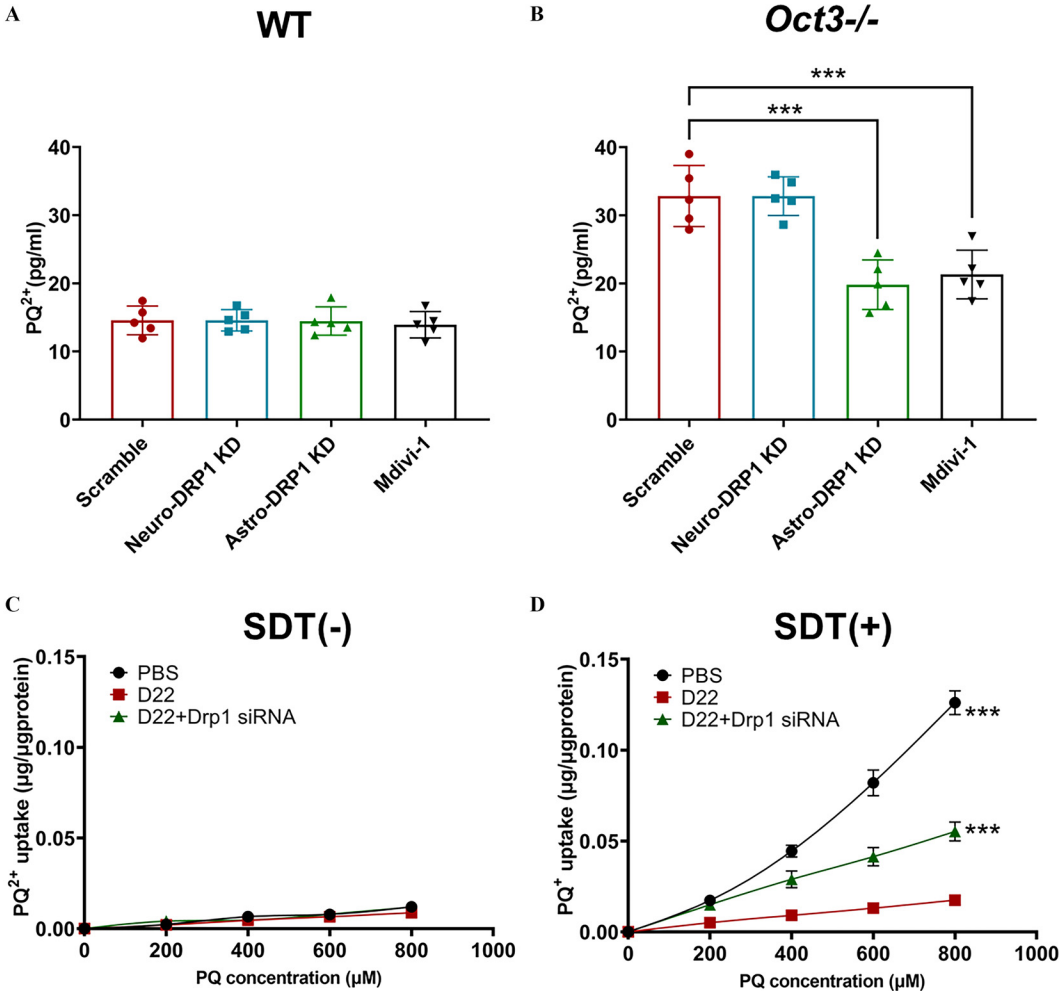

Figure 5. Evaluations of PQ^{2+} or PQ^{+} clearance in the brains of mice and in cultured astrocytes with or without DRP1 knockdown. (A,B) *In vivo* extracellular residue of the loading PQ^{2+} (PQ^{2+}-LT) was detected by microdialysis followed by HPLC in WT (A) and *Oct3*$^{-/-}$ (B) mice treated with either empty AAV control, neuronal DRP knockdown by AAV, astrocyte DRP1 knockdown by AAV, or non-selective DRP1 knockdown using mdivi-1. $n = 5$ mice per group. One-way ANOVA was followed by the Bonferroni multiple comparison test. Data are shown as mean ± SD. (C,D) PQ^{2+} or PQ^{+} uptake assays of GL261 astrocytes without or with SDT. PQ^{2+}/PQ^{+} concentration in the extracellular culture medium ranged from 0 to 800 μM (*x*-axis), and the uptake level of PQ^{2+}/PQ^{+} into astrocytes were detected in the cell lysate (*y*-axis). Drp-1 siRNA was used to knockdown DRP1 in GL261 astrocytes. The average area under the curves were calculated and used for statistical analysis. $n = 6$ independent experiments per group. One-way ANOVA was followed by the Bonferroni multiple comparison test. Data are shown as mean ± SEM. **, $p < 0.01$; ***, $p < 0.001$. The numeric data are shown in Excel Table S5. Note: AAV, adeno-associated virus; ANOVA, analysis of variance; Astro-DRP1 KD, DRP1 knockdown in astrocytes by AAV with gfaABC1D promoter; DRP1, dynamic related protein-1; HPLC, high-performance liquid chromatography; LT, loading treatment; mdivi-1, mitochondrial division inhibitor-1; Neuro-DRP1 KD, DRP1 knockdown in neuron by AAV with hsyn promoter; oct3, organic cation transporter-3; PQ, paraquat; Scramble, empty AAV for control; SD, standard deviation; SDT, sodium dithionite; SEM, standard error of the mean; siRNA, small interfering RNA; WT, wild-type.

neurons in the brains of mice.[46,47] Furthermore, research in human and rodents reported that some compounds such as tetraisoquinolines and beta-carbolines present in our diets were linked to PD onset,[48,49] and all of them structurally resembled organic cations. It was critical to discover how these cations were transported between cells in the brain, so that we could understand the pathogenic mechanisms of environmentally associated PD.

In experimental studies, PQ^{2+} has been used to model the pathology of PD, including the loss of TH-positive neurons and locomotor deficiency.[50] When PQ^{2+} reaches the nigrostriatal system after systemic injection in mice, it is converted to PQ^{+}, a substrate for both OCT3 and DAT,[19] suggesting opportunities for crosstalk between glia and DA neurons in PQ^{+} transportation. In the brain, OCT3 is mainly expressed on astrocytes, a finding based on experiments using astrocytes of human and rodents.[51] Our previous experimental studies have revealed that neurodegeneration induced by PQ^{2+} chronic treatment was more severe in *Oct3*$^{-/-}$ mice compared with WT ones, suggesting a protective effect of OCT3 in PQ^{2+}-induced neurodegeneration.[21] However, it was unknown how OCT3 expression and functions would change during the process of neurodegeneration. In the present study, we found that OCT3 expression differed throughout the process of aging and PQ^{2+}-induced neurodegeneration, as protein levels were lower with older mice and PQ^{2+}-treated mice. The lower expression of OCT3 protein could be related to compromised PQ^{2+} clearance, which, we argue, should be a target of the disease-modifying therapy. A genome-wide association study about PD also has reported that the single nucleotide polymorphism (SNP) disturbing the expression of OCT3 was related to a higher risk of PD.[52] This evidence indicates that OCT3 deficit is probably a clinical risk factor of PD onset that had not previously been recognized. To our best knowledge, the present study provides the first link between the transporting mechanisms of paraquat in *Oct3*$^{-/-}$ mice and PD-related behavioral phenotype,

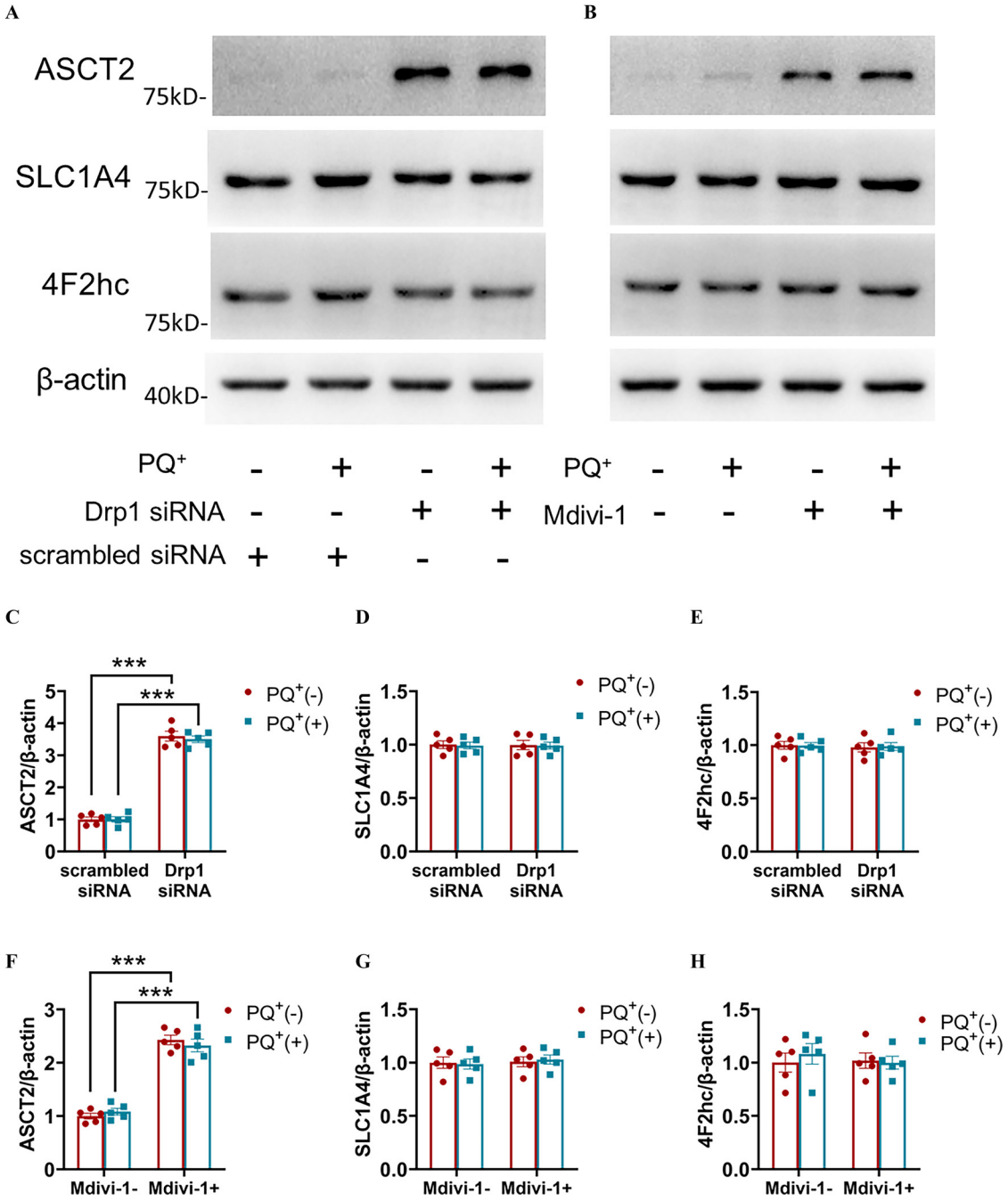

Figure 6. The levels of PQ^+ transporters in cultured astrocytes with or without DRP1 knockdown exposed to control or PQ^+. (A,B) Representative images of Western blots showing three major monovalent cation transporters in GL261 astrocytes with or without DRP1 inhibition by Drp1 siRNA or mdivi-1. Scrambled siRNA was used as control for Drp1 siRNA exposed to control or PQ^+. (C–H) Quantitative analysis of the relative expression of the transporters shown in A and B. The group of PQ^+ (–) scramble siRNA were normalized to 1. $n = 5$ independent experiments. Data are shown as mean ± SEM. Two-way ANOVA followed by the Bonferroni multiple comparison test. ***, $p < 0.001$. The numeric data are shown in Excel Table S6. In two-way ANOVAs, "*" was used to present the statistical difference between groups both treated by PBS or PQ^{2+}. Note: 4F2hc, 4F2 heavy chain of L-type amino acid transporter 1; ANOVA, analysis of variance; ASCT2, alanine serine cysteine transporter 2; DRP1, dynamic related protein-1; mdivi-1, mitochondrial division inhibitor-1; PBS, phosphate-buffered saline; PQ, paraquat; Scramble, empty AAV for control; SEM, standard error of the mean; siRNA, small interfering RNA; SLC1A4, solute carrier family 1 member 4.

which manifests as dyskinesia. In behavior tests, rotarod and gait analysis were used to assess the severity of movement disorders. Mice with dyskinesia tended to fall from the rotarod and thus had lower duration than normal mice. These mice also had abnormal gait, manifesting as shorter stride length, longer stand, and slower swing speed. It was proved that PQ^{2+} induces neuronal death through oxidative stress and ROS.[9] The lack of an assay for ROS or oxidative defense is a limitation of this study; however, because we focused on the relationship between paraquat transportation and PD phenotype, we used the damages of TH-positive neurons and animal behavior phenotypes to bridge this gap and reflect the effects of paraquat.

The PQ^{2+}-induced neurotoxic model used in the present study has been acknowledged in other *in vivo* studies on PD.[19,30] During the process of chronic treatment, PQ^{2+} was injected i.p. into mice. We acknowledge that i.p. injection is not as close to

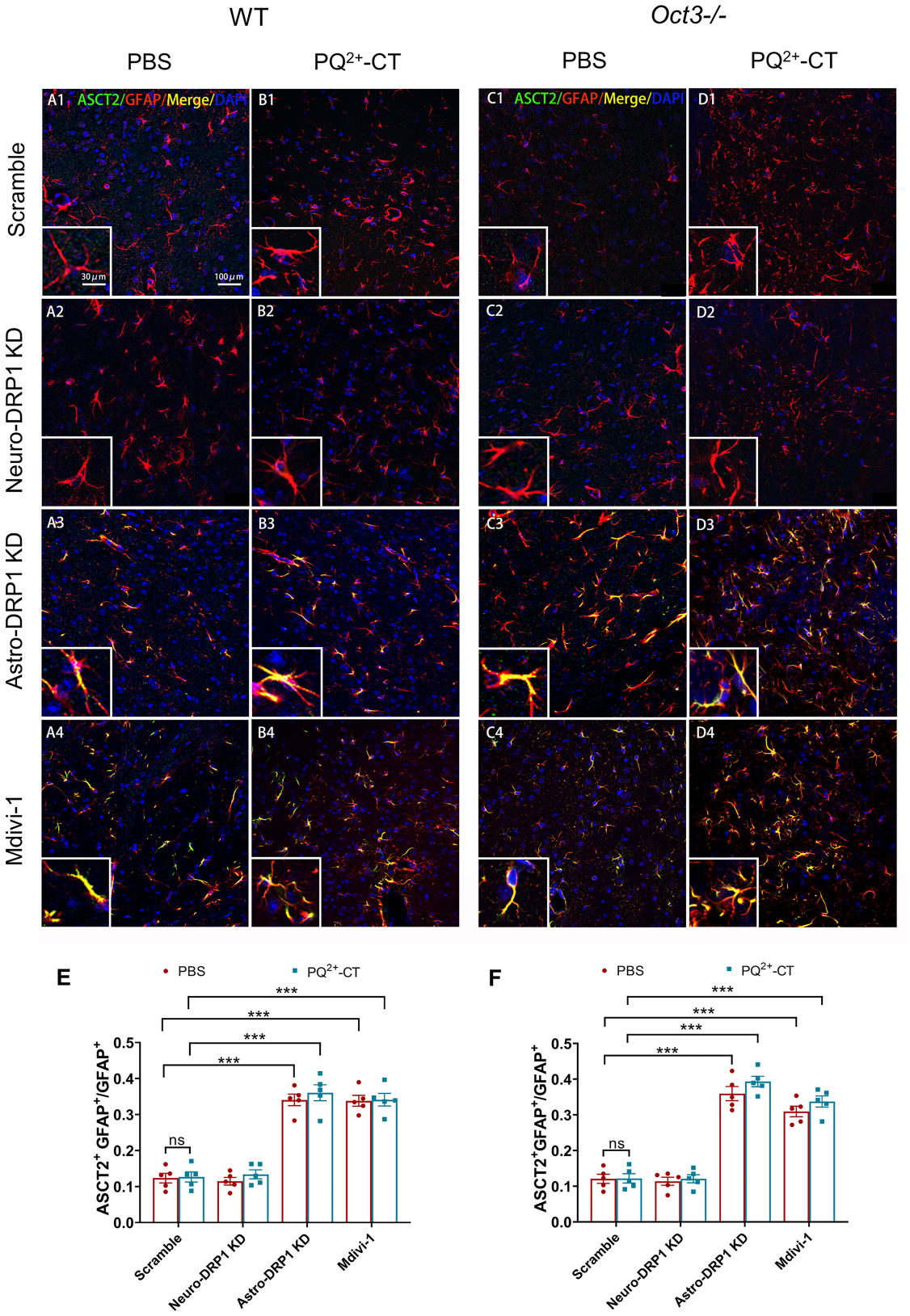

Figure 7. The expression and distribution of ASCT2 in the brains of mice. Immunofluorescent staining of ASCT2 and GFAP in the striatum of (A,B) WT mice and (C,D) *Oct3*$^{-/-}$ mice. (E,F) GFAP^{+} and ASCT2^{+}GFAP^{+} cells were counted, the proportion of ASCT2^{+}GFAP^{+}/GFAP^{+} was calculated for analysis ($n=5$ mice per group, six to eight sections were analyzed per mouse. The average value per mouse was used for statistics). Data are shown as the mean ± SEM. Two-way ANOVA followed by the Bonferroni multiple comparison test. ***, $p<0.001$, ns, no significance. The numeric data are shown in Excel Table S7. Note: ANOVA, analysis of variance; ASCT2, alanine serine cysteine transporter 2; Astro-DRP1 KD, DRP1 knockdown in astrocytes by AAV with gfaABC1D promoter; DRP1, dynamic related protein-1; GFAP, glial fibrillary acidic protein; mdivi-1, mitochondrial division inhibitor-1; OCT3; organic cation transporter-3; PBS, phosphate-buffered saline; PQ, paraquat; Neuro-DRP1 KD, DRP1 knockdown in neuron by AAV with hsyn promoter; Scramble, empty AAV for control; SEM, standard error of the mean; WT, wild-type.

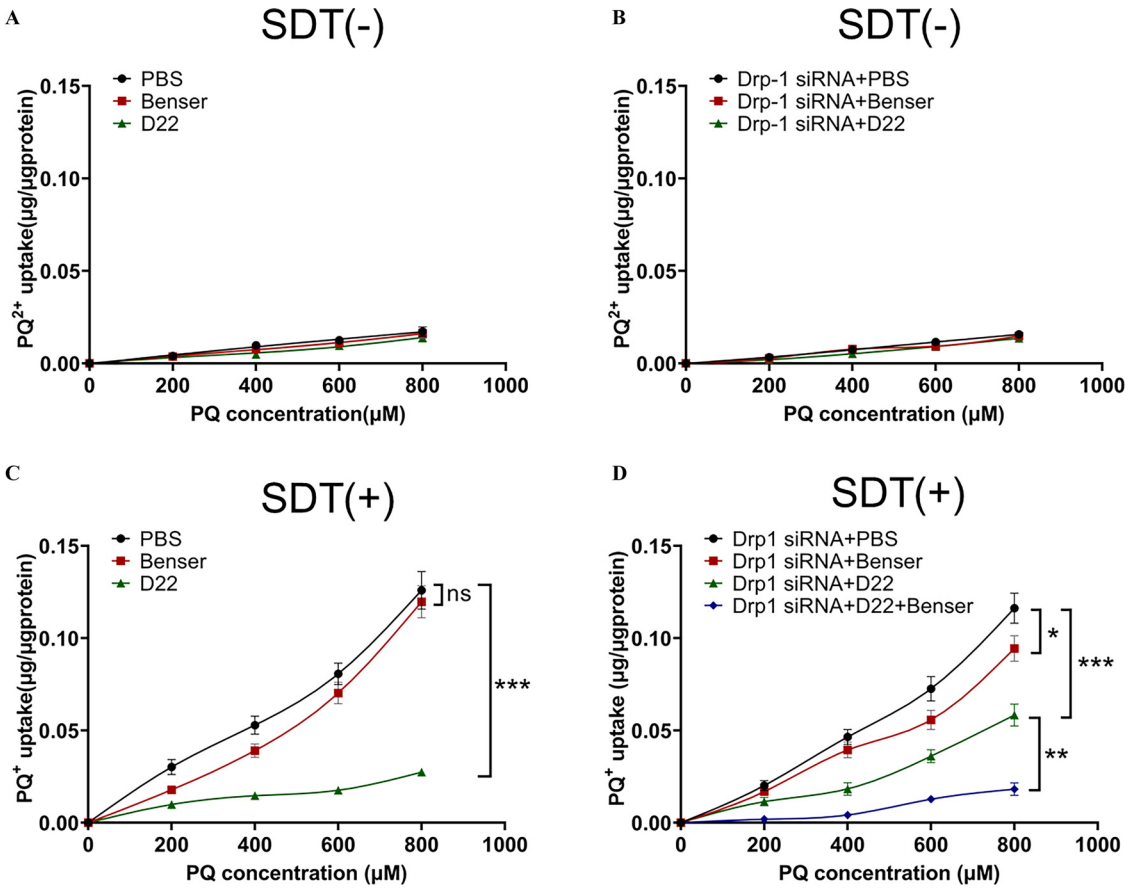

Figure 8. Transport of PQ^{2+} or PQ^{+} into the GL261 astrocyte cell line with and without specific inhibitors of ASCT2 and OCT3, with and without siRNA targeting Drp-1. PQ^{+}/PQ^{2+} (with or without SDT) transportation into GL261 astrocytes was evaluated using *in vitro* uptake assay. Specific inhibitors (Benser for ASCT2; D22 for OCT3) were used to evaluate the role of ASCT2 and OCT3, respectively. (A,B) The intake capacity of PQ^{2+} by GL261 astrocytes without (A) or with (B) Drp1 siRNA. The average area under the curve was used for statistical analysis. $n = 6$ independent experiments. (C,D) The intake capacity of PQ^{+} (PQ^{2+} pretreated with SDT) by GL261 astrocytes without (C) or with (D) Drp1 siRNA. Area under the curve was analyzed. $n = 6$ independent experiments. PQ^{2+}/PQ^{+} concentrations in extracellular culture medium ranged from 0 to 800 μM (*x*-axis). The intake PQ^{2+}/PQ^{+} was detected in the cell lysate (*y*-axis). Data are shown as the mean ± SEM. One-way ANOVA was followed by the Bonferroni multiple comparison test. *, $p < 0.01$; ***, $p < 0.001$. The numeric data are shown in Excel Table S8. Note: ANOVA, analysis of variance; ASCT2, alanine serine cysteine transporter 2; Benser, benzylserine; D22, Decynium 22; DRP1, dynamic related protein-1; OCT3, organic cation transporter-3; PBS, phosphate-buffered saline; PQ, paraquat; SDT, sodium dithionite; SEM, standard error of the mean; siRNA, small interfering RNA.

the real-world exposure as other methods, including inhalation or gavage. However, an i.p. injection was the most feasible method to use the least dosage and ensure that each mouse received an equivalent dose of PQ^{2+} in such a way that extracellular PQ^{2+} measurements by *in vivo* microdialysis were comparable, given that we mainly focused on the transport mechanisms of PQ^{2+} in the brain. It was reported that inhalation and gavage of PQ^{2+} were not efficient enough to model the PD symptoms but, rather, caused pulmonary fibrosis in mice.[53–56] The method of gavage has been usually used to model acute lung injury, pulmonary fibrosis and liver damage in mice.[57–59] Only a few studies in rodents used gavage PQ^{2+} to model PD symptoms, but usually in a larger dose (such as 10 mg/kg/d for 28 d)[60] or supplemented with another drug.[61] These studies observed the pathology of PD in the brain but did not detect the cerebral extracellular level of PQ^{2+}, which could be influenced by absorption in the digestive system. Moreover, the dosage of PQ^{2+} in the present study has been commonly used in similar mouse studies about PD.[18,30] In the real world, although epidemiological studies have revealed the relationship between PQ exposure and PD onset, the PQ^{2+} levels in the brains of exposed population are still unknown[16] and difficult to detect. Thus, no "standard concentration" could be considered in experimental studies to mimic the PQ exposure in the real world. The dosage in the present study (10 mg/kg) was probably higher than in the real-world exposure, but it was lower than other methods used in experimental studies, such as gavage. Despite this "overload" exposure, the pathology of PD could only be mimicked subclinically, with loss of TH-positive neurons but sparing of striatal terminals. We assumed that human beings and rodents might have different sensitivities to PQ. It remained to be explored how to better mimic the real-world exposure of PQ in rodent models. The PQ dosages we used to treat the cells were used in previous *in vitro* studies.[30,62] However, in the present study, cells were not continuously incubated in reported concentrations of PQ. A short incubation time of 20 min was adopted, after which the PQ was replaced by normal culture medium so that we could observe uptake activities during this period of time and the effects of PQ intake to the cells. The PQ taken up by the cells represented only a small portion of the PQ in the culture medium in the present study. DRP1 has been acknowledged as a key regulator of mitochondrial fission based on research on rodents and cells.[26] Excessive elevation of DRP1 exacerbated mitochondrial fragmentation, accelerating the apoptosis of cells in a nonhuman primate.[63] Recently, the roles of DRP1 in astrocytes have been gradually revealed. For example, DRP1 could regulate the activation of astrocytes and mediate the inflammatory

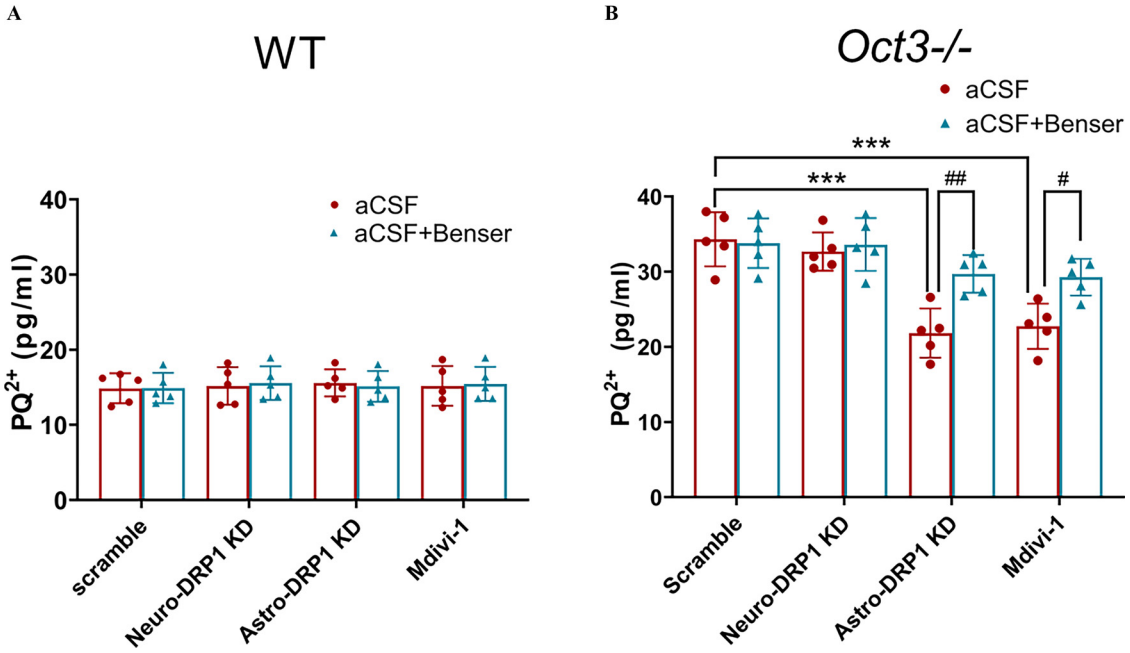

Figure 9. The extracellular residue of the loading dose of PQ^{2+} in the brains of mice with or without Benser treatment. The extracellular PQ^{2+} levels in (A) WT and (B) $Oct3^{-/-}$ mice with or without infusion of aCSF containing Benser were measured ($n = 5$ mice per group). Data are shown as the mean ± SD. Two-way ANOVAs were followed by the Bonferroni multiple comparison test. #, $p < 0.05$; ##, $p < 0.01$; ***/###, $p < 0.001$. The numeric data are shown in Excel Table S9. In two-way ANOVAs, "*" was used to present the statistical difference between groups both treated by normal aCSF, and "#" was used to present the statistical difference between groups treated by aCSF with or without Benser. Note: aCSF, artificial cerebrospinal fluid; ANOVA, analysis of variance; Astro-DRP1 KD, DRP1 knockdown in astrocytes by AAV with gfaABC1D promoter; DRP1, dynamic related protein-1; mdivi-1, mitochondrial division inhibitor-1; OCT3, organic cation transporter-3; PQ, paraquat; Neuro-DRP1 KD, DRP1 knockdown in neuron by AAV with hsyn promoter; Scramble, empty AAV for control; SD, standard deviation; WT, wild-type.

reactions related to astrocytes in the brains of mice.[29] In the present study, we found that astrocyte DRP1 protein expression could be stimulated by PQ^{2+}-CT. Selective astrocyte DRP1 knockdown significantly relieved the PQ^{2+}-induced neurotoxicity, but these protective effects were only observed in $Oct3^{-/-}$ mice. As we discussed above, $Oct3^{-/-}$ mice were less able transport extracellular PQ^{2+} into astrocytes,[21] which led us to speculate whether DRP1 knockdown in astrocytes could restore a compromised process of PQ clearance. *In vivo* microdialysis showed that extracellular residue of the loading PQ^{2+} was lower in the striatum of $Oct3^{-/-}$ mice receiving astrocyte DRP1 knockdown, suggesting restored PQ^{2+} clearance and transport in the nigrostriatal system of mice. Through *in vitro* experiments, we directly measured the higher levels of PQ^{+} transport in astrocytes after treatment of Drp1 siRNA. Furthermore, increased PQ^{+} transport induced by astrocyte DRP1 knockdown was related to the higher expression of ASCT2, one of the PQ^{+} transporters mainly distributed in astrocytes.[64] The function of this transporter was further evaluated by *in vitro* transport studies. We found that PQ^{2+} was a poor substrate for both OCT3 and ASCT2 until reduced to PQ^{+}. Interestingly, OCT3 had a much higher affinity than ASCT2, combined with the low endogenous level of ASCT2, which might explain the limited functions of ASCT2 in WT mice under physiological conditions. However, when OCT3 protein levels were lower during aging or chronic toxic exposure, ASCT2 could function as an alternative transporter to compensate for its role, contributing to the continuous clearance of extracellular PQ^{2+}. Taken together, we established here the relationships between astrocyte DRP1 and PQ^{2+}-induced neurotoxicity. In particular, we revealed a complementary pathway to restore PQ clearance in the brains of mice with OCT3 deficiency. In environmentally pathogenic PD, the function of glia surrounding DA neurons including astrocytes is crucial for the microenvironment of the nigrostriatal system and the survival of DA neurons. Interfering with the transporters located on these astrocytes may bring more benefits than just regulating neuronal function. Our research suggests that DRP1 could be one of the potential targets of modifying therapies for PD. In addition to the amelioration of mitochondrial fragmentation,[65] astrocyte DRP1 inhibition was also involved in the regulation of toxin transport, one of the critical causes of environmentally pathogenic Parkinson's disease.[66] As discussed above, ASCT2 was up-regulated by selective astrocyte DRP1 inhibition. However, the underlying mechanisms require further elucidation. Mitochondrial retrograde signaling is suggested to be a potential pathway.[67] The influence of DRP1 on mitochondrial functions could regulate the expression of nuclear-encoded proteins, enabling communication between mitochondrial activities and the intracellular protein expression system, which has been reported in studies of drosophila and animal cells.[68,69] The modified nuclear-encoded proteins consist of different transporters on the cell membrane related to amino acid metabolism.[70] Pathways including the mammalian target of rapamycin (mTOR) and nuclear factor kappa B (NF-κB) are involved in these responses.[71,72] The results in the present study enrich our knowledge on astrocyte DRP1 and substantiate that cultivating mitochondrial fission is not the only function of DRP1.

In the present study, mdivi-1 was revealed to ameliorate PQ^{2+}-induced neurodegeneration in both WT and $Oct3^{-/-}$ mice. A similar protective effect of mdivi-1 in both genotypes could be related to its lipophilic and small molecular structure, making it possible to freely pass through the blood–brain barrier[38] and non-selectively regulate mitochondrial fission/fusion in the neurons[73] and astrocytes.[74] Recently, ROS production and oxidative stress have also been reported to be the targets of mdivi-1 *in vitro*.[75] This small molecule could be a promising molecular target for

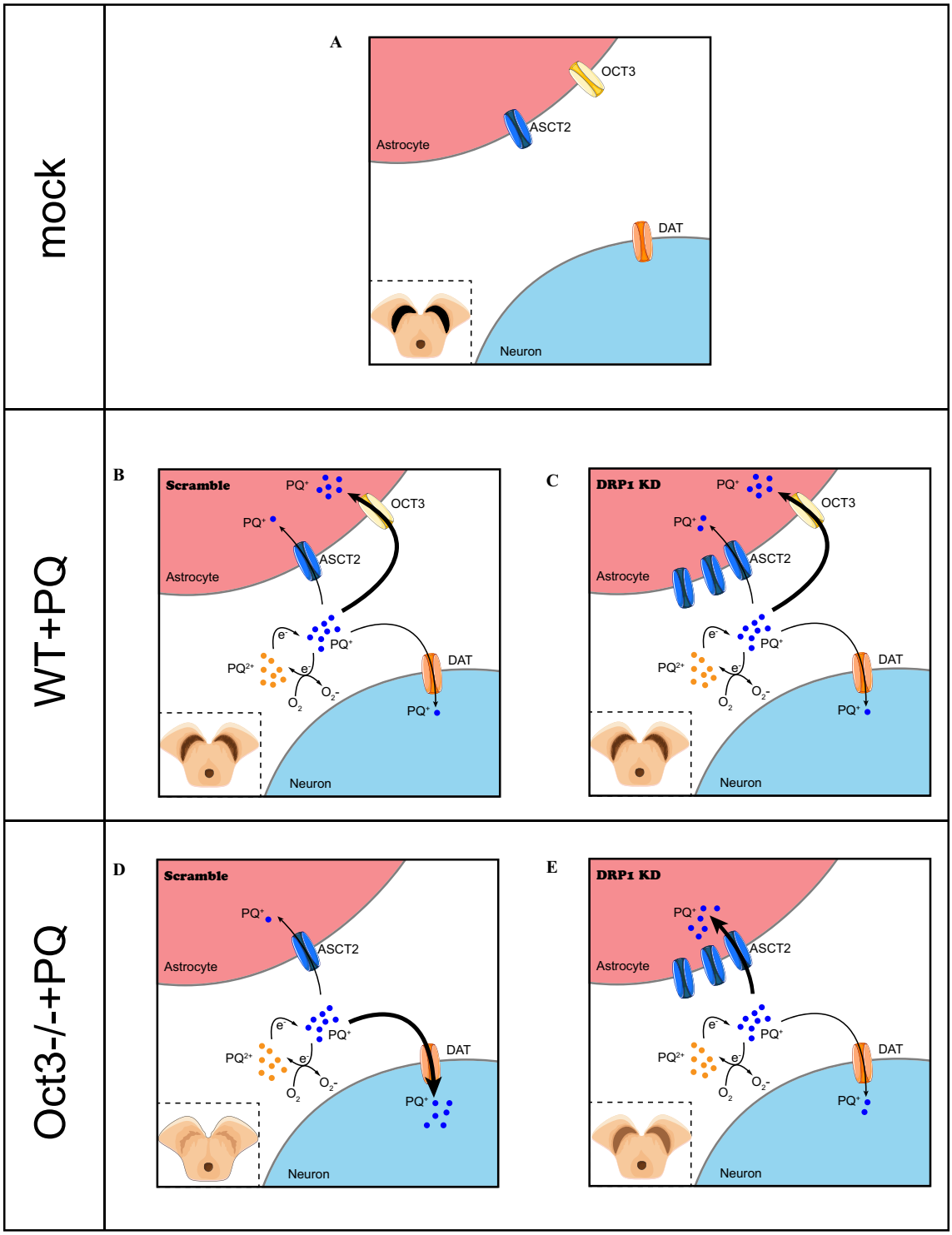

Figure 10. Schematic diagram summarizing the present study. (A) In the brains of mice, ASCT2 and OCT3 transporters were both expressed on astrocytes, and DAT was expressed on DA neurons. (B) PQ^{2+} could be reduced to PQ^{+}, which acted as a substrate of OCT3, DAT, and ASCT2. In WT mice, most PQ^{+} was transported by OCT3 into astrocytes; only a small portion of PQ^{+} was transported by DAT into neurons, which we predict was related to the incomplete PD phenotype. Here, "incomplete PD phenotype" indicates a milder lesion of the dopaminergic neuron compared with the classical PD pathology, accompanied by uninfluenced dopamine release and behavior performance. ASCT2 had limited function in PQ^{+} transportation here. (C) When astrocyte DRP1 was knocked down in WT mice using miRNA AAV, although the protein level of ASCT2 was higher than in mice treated with the scramble AAV, PQ transported by ASCT2 was not significantly different, likely due to the higher transporting activity of OCT3 than ASCT2 in astrocytes. In addition, the severity of the PD phenotype was not influenced by astrocyte DRP1 knockdown. (D) In $Oct3^{-/-}$ mice, more PQ^{+} was transported into neurons by DAT than in WT mice, likely due to the absence of the high affinity OCT3. We found that ASCT2, which was expressed at a low level and with weak transporting activity, could not compensate for the loss of OCT3; we predict this was the reason for the significant aggravation of PD phenotype in $Oct3^{-/-}$ mice. (E) When astrocyte DRP1 was knocked down in $Oct3^{-/-}$ mice using miRNA AAV, ASCT2 was expressed at a higher level than in mice treated with the scramble AAV. These mice also transported more PQ (mostly PQ^{+}) into astrocytes, thus limiting the amount of PQ^{+} transported by DAT into neurons, which we predict was related to the relieved PD phenotype. Note: AAV, adeno-associated virus; ANOVA, analysis of variance; ASCT2, alanine serine cysteine transporter 2; DA, dopamine; DAT, dopamine transporter; DRP1, dynamic related protein-1; OCT3, organic cation transporter-3; PD, Parkinson's disease; PQ, paraquat; Scramble, empty AAV for control; WT, wild-type.

the disease-modifying treatment of environmentally pathogenic Parkinson's disease.

In summary, the present study highlights the existence of a complementary pathway modulated by astrocyte DRP1 during PQ^{2+}-induced neurodegeneration through coordinated interactions of astrocytes and DA terminals. Our study revealed that OCT3, ASCT2 located on astrocytes, and DAT located on DA terminals might function in a coordinated manner to mediate the susceptibility to toxicity induced by PQ. The conclusions of the present study are summarized in Figure 10. By extension, other monovalent cation toxicants might also share the same mechanisms; accordingly, this present study provides the basis for future studies investigating the effect of neurotoxicity on the nigrostriatal pathway.

Acknowledgments

M.C., Yx.Z, and Q.D. determined the subject direction and designed the research. S.H. and Y.F. completed experiments and wrote the manuscript. M.G. helped with the experiment design, figure preparation, data analysis, draft writing and manuscript revision. Y.H. and J.S. helped complete the *in vivo* experiments and modified the manuscript. Yc.Z. helped complete the *in vitro* experiments and analyzed data.

We thank K. Tieu (Florida International University) for providing us with the *Oct3*$^{-/-}$ mice. The institute of Neurology of Fudan University provided the experimental platform for this study.

Funding for this work was provided by the National Natural Science Foundation of China (81971013 to M.C., 82071197 to Q.D., and 82101336 to M.G.) and by the Science and Technology Commission of Shanghai Municipality (20ZR1443500 to Yx.Z).

References

1. Smith P, Heath D, Fishman AP. 1976. Paraquat. CRC Crit Rev Toxicol 4(4):411–445, PMID: 791582, https://doi.org/10.1080/10408447609164020.
2. Bromilow RH. 2004. Paraquat and sustainable agriculture. Pest Manag Sci 60(4):340–349, PMID: 15119596, https://doi.org/10.1002/ps.823.
3. Damalas CA, Eleftherohorinos IG. 2011. Pesticide exposure, safety issues, and risk assessment indicators. Int J Environ Res Public Health 8(5):1402–1419, PMID: 21655127, https://doi.org/10.3390/ijerph8051402.
4. Kumar S, Gupta S, Bansal YS, Bal A, Rastogi P, Muthu V, et al. 2021. Pulmonary histopathology in fatal paraquat poisoning. Autops Case Rep 11:e2021342, PMID: 34926332, https://doi.org/10.4322/acr.2021.342.
5. Richardson JR, Fitsanakis V, Westerink RHS, Kanthasamy AG. 2019. Neurotoxicity of pesticides. Acta Neuropathol 138(3):343–362, PMID: 31197504, https://doi.org/10.1007/s00401-019-02033-9.
6. George B, You D, Joy MS, Aleksunes LM. 2017. Xenobiotic transporters and kidney injury. Adv Drug Deliv Rev 116:73–91, PMID: 28111348, https://doi.org/10.1016/j.addr.2017.01.005.
7. Nandipati S, Litvan I. 2016. Environmental exposures and Parkinson's disease. Int J Environ Res Public Health 13(9):881, PMID: 27598189, https://doi.org/10.3390/ijerph13090881.
8. Ascherio A, Schwarzschild MA. 2016. The epidemiology of Parkinson's disease: risk factors and prevention. Lancet Neurol 15(12):1257–1272, PMID: 27751556, https://doi.org/10.1016/S1474-4422(16)30230-7.
9. Baltazar MT, Dinis-Oliveira RJ, de Lourdes Bastos M, Tsatsakis AM, Duarte JA, Carvalho F. 2014. Pesticides exposure as etiological factors of Parkinson's disease and other neurodegenerative diseases—a mechanistic approach. Toxicol Lett 230(2):85–103, PMID: 24503016, https://doi.org/10.1016/j.toxlet.2014.01.039.
10. Cochemé HM, Murphy MP. 2008. Complex I is the major site of mitochondrial superoxide production by paraquat. J Biol Chem 283(4):1786–1798, PMID: 18039652, https://doi.org/10.1074/jbc.M708597200.
11. McCormack AL, Atienza JG, Johnston LC, Andersen JK, Vu S, Di Monte DA. 2005. Role of oxidative stress in paraquat-induced dopaminergic cell degeneration. J Neurochem 93(4):1030–1037, PMID: 15857406, https://doi.org/10.1111/j.1471-4159.2005.03088.x.
12. Reczek CR, Birsoy K, Kong H, Martínez-Reyes I, Wang T, Gao P, et al. 2017. A CRISPR screen identifies a pathway required for paraquat-induced cell death. Nat Chem Biol 13(12):1274–1279, PMID: 29058724, https://doi.org/10.1038/nchembio.2499.
13. Zhao G, Cao K, Xu C, Sun A, Lu W, Zheng Y, et al. 2017. Crosstalk between mitochondrial fission and oxidative stress in paraquat-induced apoptosis in mouse alveolar type II cells. Int J Biol Sci 13(7):888–900, PMID: 28808421, https://doi.org/10.7150/ijbs.18468.
14. Bastías-Candia S, Zolezzi JM, Inestrosa NC. 2019. Revisiting the paraquat-induced sporadic Parkinson's disease-like model. Mol Neurobiol 56(2):1044–1055, PMID: 29862459, https://doi.org/10.1007/s12035-018-1148-z.
15. Manning-Bog AB, McCormack AL, Li J, Uversky VN, Fink AL, Di Monte DA. 2002. The herbicide paraquat causes up-regulation and aggregation of alpha-synuclein in mice: paraquat and alpha-synuclein. J Biol Chem 277(3):1641–1644, PMID: 11707429, https://doi.org/10.1074/jbc.C100560200.
16. Tanner CM, Kamel F, Ross GW, Hoppin JA, Goldman SM, Korell M, et al. 2011. Rotenone, paraquat, and Parkinson's disease. Environ Health Perspect 119(6):866–872, PMID: 21269927, https://doi.org/10.1289/ehp.1002839.
17. Zeng XS, Geng WS, Jia JJ. 2018. Neurotoxin-induced animal models of Parkinson disease: pathogenic mechanism and assessment. ASN Neuro 10:1759091418777438, PMID: 29809058, https://doi.org/10.1177/1759091418777438.
18. McCormack AL, Thiruchelvam M, Manning-Bog AB, Thiffault C, Langston JW, Cory-Slechta DA, et al. 2002. Environmental risk factors and Parkinson's disease: selective degeneration of nigral dopaminergic neurons caused by the herbicide paraquat. Neurobiol Dis 10(2):119–127, PMID: 12127150, https://doi.org/10.1006/nbdi.2002.0507.
19. Rappold PM, Cui M, Chesser AS, Tibbett J, Grima JC, Duan L, et al. 2011. Paraquat neurotoxicity is mediated by the dopamine transporter and organic cation transporter-3. Proc Natl Acad Sci U S A 108(51):20766–20771, PMID: 22143804, https://doi.org/10.1073/pnas.1115141108.
20. Thiruchelvam M, McCormack A, Richfield EK, Baggs RB, Tank AW, Di Monte DA, et al. 2003. Age-related irreversible progressive nigrostriatal dopaminergic neurotoxicity in the paraquat and maneb model of the Parkinson's disease phenotype. Eur J Neurosci 18(3):589–600, PMID: 12911755, https://doi.org/10.1046/j.1460-9568.2003.02781.x.
21. Cui M, Aras R, Christian WV, Rappold PM, Hatwar M, Panza J, et al. 2009. The organic cation transporter-3 is a pivotal modulator of neurodegeneration in the nigrostriatal dopaminergic pathway. Proc Natl Acad Sci U S A 106(19):8043–8048, PMID: 19416912, https://doi.org/10.1073/pnas.0900358106.
22. Bonneh-Barkay D, Reaney SH, Langston WJ, Di Monte DA. 2005. Redox cycling of the herbicide paraquat in microglial cultures. Brain Res Mol Brain Res 134(1):52–56, PMID: 15790529, https://doi.org/10.1016/j.molbrainres.2004.11.005.
23. Wu XF, Block ML, Zhang W, Qin L, Wilson B, Zhang WQ, et al. 2005. The role of microglia in paraquat-induced dopaminergic neurotoxicity. Antioxid Redox Signal 7(5–6):654–661, PMID: 15890010, https://doi.org/10.1089/ars.2005.7.654.
24. Lee WK, Wolff NA, Thévenod F. 2009. Organic cation transporters: physiology, toxicology and special focus on ethidium as a novel substrate. Curr Drug Metab 10(6):617–631, PMID: 19702534, https://doi.org/10.2174/138920009789375360.
25. Richter F, Gabby L, McDowell KA, Mulligan CK, De La Rosa K, Sioshansi PC, et al. 2017. Effects of decreased dopamine transporter levels on nigrostriatal neurons and paraquat/maneb toxicity in mice. Neurobiol Aging 51:54–66, PMID: 28038352, https://doi.org/10.1016/j.neurobiolaging.2016.11.015.
26. Qi Z, Huang Z, Xie F, Chen L. 2019. Dynamin-related protein 1: a critical protein in the pathogenesis of neural system dysfunctions and neurodegenerative diseases. J Cell Physiol 234(7):10032–10046, PMID: 30515821, https://doi.org/10.1002/jcp.27866.
27. Filichia E, Hoffer B, Qi X, Luo Y. 2016. Inhibition of Drp1 mitochondrial translocation provides neural protection in dopaminergic system in a Parkinson's disease model induced by MPTP. Sci Rep 6:32656, PMID: 27619562, https://doi.org/10.1038/srep32656.
28. Zhang X, Huang W, Shao Q, Yang Y, Xu Z, Chen J, et al. 2020. Drp1, a potential therapeutic target for Parkinson's disease, is involved in olfactory bulb pathological alteration in the rotenone-induced rat model. Toxicol Lett 325:1–13, PMID: 32088201, https://doi.org/10.1016/j.toxlet.2020.02.009.
29. Wu X, Luo J, Liu H, Cui W, Guo K, Zhao L, et al. 2020. Recombinant adiponectin peptide ameliorates brain injury following intracerebral hemorrhage by suppressing astrocyte-derived inflammation via the inhibition of Drp1-mediated mitochondrial fission. Transl Stroke Res 11(5):924–939, PMID: 31902083, https://doi.org/10.1007/s12975-019-00768-x.
30. Zhang Y, Shao W, Wu J, Huang S, Yang H, Luo Z, et al. 2021. Inflammatory lncRNA AK039862 regulates paraquat-inhibited proliferation and migration of microglial and neuronal cells through the Pafah1b1/Foxa1 pathway in co-culture environments. Ecotoxicol Environ Saf 208:111424, PMID: 33120262, https://doi.org/10.1016/j.ecoenv.2020.111424.
31. Brooks AI, Chadwick CA, Gelbard HA, Cory-Slechta DA, Federoff HJ. 1999. Paraquat elicited neurobehavioral syndrome caused by dopaminergic neuron loss. Brain Res 823(1–2):1–10, PMID: 10095006, https://doi.org/10.1016/S0006-8993(98)01192-5.
32. Khwaja M, McCormack A, McIntosh JM, Di Monte DA, Quik M. 2007. Nicotine partially protects against paraquat-induced nigrostriatal damage in mice; link to $\alpha6\beta2^*$ nAChRs. J Neurochem 100(1):180–190, PMID: 17227438, https://doi.org/10.1111/j.1471-4159.2006.04177.x.

33. Liang LP, Kavanagh TJ, Patel M. 2013. Glutathione deficiency in *Gclm* null mice results in complex I inhibition and dopamine depletion following paraquat administration. Toxicol Sci 134(2):366–373, PMID: 23704229, https://doi.org/10.1093/toxsci/kft112.
34. Reeves R, Thiruchelvam M, Baggs RB, Cory-Slechta DA. 2003. Interactions of paraquat and triadimefon: behavioral and neurochemical effects. Neurotoxicology 24(6):839–850, PMID: 14637379, https://doi.org/10.1016/S0161-813X(03)00057-3.
35. Zwart R, Verhaagh S, Buitelaar M, Popp-Snijders C, Barlow DP. 2001. Impaired activity of the extraneuronal monoamine transporter system known as uptake-2 in *Orct3/Slc22a3*-deficient mice. Mol Cell Biol 21(13):4188–4196, PMID: 11390648, https://doi.org/10.1128/MCB.21.13.4188-4196.2001.
36. National Research Council Committee for the Update of the Guide for the Care and Use of Laboratory Animals. 2011. *Guide for the Care and Use of Laboratory Animals*. 8th ed. Washington, DC: National Academies Press.
37. Lackner LL, Nunnari J. 2010. Small molecule inhibitors of mitochondrial division: tools that translate basic biological research into medicine. Chem Biol 17(6):578–583, PMID: 20609407, https://doi.org/10.1016/j.chembiol.2010.05.016.
38. Rappold PM, Cui M, Grima JC, Fan RZ, de Mesy-Bentley KL, Chen L, et al. 2014. Drp1 inhibition attenuates neurotoxicity and dopamine release deficits *in vivo*. Nat Commun 5:5244, PMID: 25370169, https://doi.org/10.1038/ncomms6244.
39. Rempe DA, Lelli KM, Vangeison G, Johnson RS, Federoff HJ. 2007. In cultured astrocytes, p53 and MDM2 do not alter hypoxia-inducible factor-1α function regardless of the presence of DNA damage. J Biol Chem 282(22):16187–16201, PMID: 17420250, https://doi.org/10.1074/jbc.M702203200.
40. Freundt EC, Maynard N, Clancy EK, Roy S, Bousset L, Sourigues Y, et al. 2012. Neuron-to-neuron transmission of α-synuclein fibrils through axonal transport. Ann Neurol 72(4):517–524, PMID: 23109146, https://doi.org/10.1002/ana.23747.
41. Guo M, Wang J, Zhao Y, Feng Y, Han S, Dong Q, et al. 2020. Microglial exosomes facilitate α-synuclein transmission in Parkinson's disease. Brain 143(5):1476–1497, PMID: 32355963, https://doi.org/10.1093/brain/awaa090.
42. Samii A, Nutt JG, Ransom BR. 2004. Parkinson's disease. Lancet 363(9423):1783–1793, PMID: 15172778, https://doi.org/10.1016/S0140-6736(04)16305-8.
43. Tysnes OB, Storstein A. 2017. Epidemiology of Parkinson's disease. J Neural Transm (Vienna) 124(8):901–905, PMID: 28150045, https://doi.org/10.1007/s00702-017-1686-y.
44. Richardson JR, Quan Y, Sherer TB, Greenamyre JT, Miller GW. 2005. Paraquat neurotoxicity is distinct from that of MPTP and rotenone. Toxicol Sci 88(1):193–201, PMID: 16141438, https://doi.org/10.1093/toxsci/kfi304.
45. Langston JW. 2017. The MPTP story. J Parkinsons Dis 7(suppl 1):S11–S19, PMID: 28282815, https://doi.org/10.3233/JPD-179006.
46. Dauer W, Przedborski S. 2003. Parkinson's disease: mechanisms and models. Neuron 39(6):889–909, PMID: 12971891, https://doi.org/10.1016/S0896-6273(03)00568-3.
47. Huang CL, Chao CC, Lee YC, Lu MK, Cheng JJ, Yang YC, et al. 2016. Paraquat induces cell death through impairing mitochondrial membrane permeability. Mol Neurobiol 53(4):2169–2188, PMID: 25947082, https://doi.org/10.1007/s12035-015-9198-y.
48. Matsubara K, Aoyama K, Suno M, Awaya T. 2002. *N*-methylation underlying Parkinson's disease. Neurotoxicol Teratol 24(5):593–598, PMID: 12200190, https://doi.org/10.1016/s0892-0362(02)00212-x.
49. Piechowska P, Zawirska-Wojtasiak R, Mildner-Szkudlarz S. 2019. Bioactive β-carbolines in food: a review. Nutrients 11(4):814, PMID: 30978920, https://doi.org/10.3390/nu11040814.
50. Jackson-Lewis V, Blesa J, Przedborski S. 2012. Animal models of Parkinson's disease. Parkinsonism Relat Disord 18(suppl 1):S183–S185, PMID: 22166429, https://doi.org/10.1016/S1353-8020(11)70057-8.
51. Gasser PJ. 2021. Organic cation transporters in brain catecholamine homeostasis. Handb Exp Pharmacol 266:187–197, PMID: 33987762, https://doi.org/10.1007/164_2021_470.
52. Pankratz N, Wilk JB, Latourelle JC, DeStefano AL, Halter C, Pugh EW, et al. 2009. Genomewide association study for susceptibility genes contributing to familial Parkinson disease. Hum Genet 124(6):593–605, PMID: 18985386, https://doi.org/10.1007/s00439-008-0582-9.
53. Heydari M, Mokhtari-Zaer A, Amin F, Memarzia A, Saadat S, Hosseini M, et al. 2021. The effect of *Zataria multiflora* hydroalcoholic extract on memory and lung changes induced by rats that inhaled paraquat. Nutr Neurosci 24(9):674–687, PMID: 31583983, https://doi.org/10.1080/1028415X.2019.1668173.
54. Minnema DJ, Travis KZ, Breckenridge CB, Sturgess NC, Butt M, Wolf JC, et al. 2014. Dietary administration of paraquat for 13 weeks does not result in a loss of dopaminergic neurons in the *substantia nigra* of C57BL/6J mice. Regul Toxicol Pharmacol 68(2):250–258, PMID: 24389362, https://doi.org/10.1016/j.yrtph.2013.12.010.
55. Mirazee S, Mansouri E, Shirani M, Zeinvand-Lorestani M, Khodayar MJ. 2019. Diosmin ameliorative effects on oxidative stress and fibrosis in paraquat-induced lung injury in mice. Environ Sci Pollut Res Int 26(36):36468–36477, PMID: 31732951, https://doi.org/10.1007/s11356-019-06572-2.
56. Rojo AI, Cavada C, de Sagarra MR, Cuadrado A. 2007. Chronic inhalation of rotenone or paraquat does not induce Parkinson's disease symptoms in mice or rats. Exp Neurol 208(1):120–126, PMID: 17880941, https://doi.org/10.1016/j.expneurol.2007.07.022.
57. Luan RL, Meng XX, Jiang W. 2016. Protective effects of apigenin against paraquat-induced acute lung injury in mice. Inflammation 39(2):752–758, PMID: 26782361, https://doi.org/10.1007/s10753-015-0302-2.
58. Rao SS, Zhang XY, Shi MJ, Xiao Y, Zhang YY, Wang YY, et al. 2016. Suberoylanilide hydroxamic acid attenuates paraquat-induced pulmonary fibrosis by preventing Smad7 from deacetylation in rats. J Thorac Dis 8(9):2485–2494, PMID: 27747000, https://doi.org/10.21037/jtd.2016.08.08.
59. Tavakol HS, Farzad K, Fariba M, Abdolkarim C, Hassan G, Seyed-Mostafa HZ, et al. 2015. Hepatoprotective effect of *Matricaria chamomilla.L* in paraquat induced rat liver injury. Drug Res (Stuttg) 65(2):61–64, PMID: 24696426, https://doi.org/10.1055/s-0033-1363999.
60. Lou D, Wang Q, Huang M, Zhou Z. 2016. Does age matter? Comparison of neurobehavioral effects of paraquat exposure on postnatal and adult C57BL/6 mice. Toxicol Mech Methods 26(9):667–673, PMID: 27687147, https://doi.org/10.1080/15376516.2016.1223241.
61. Anselmi L, Bove C, Coleman FH, Le K, Subramanian MP, Venkiteswaran K, et al. 2018. Ingestion of subthreshold doses of environmental toxins induces ascending parkinsonism in the rat. NPJ Parkinsons Dis 4:30, PMID: 30302391, https://doi.org/10.1038/s41531-018-0066-0.
62. Yu Q, Wang T, Zhou X, Wu J, Chen X, Liu Y, et al. 2011. Wld^S reduces paraquat-induced cytotoxicity via SIRT1 in non-neuronal cells by attenuating the depletion of NAD. PLoS One 6(7):e21770, PMID: 21750730, https://doi.org/10.1371/journal.pone.0021770.
63. Park J, Seo J, Won J, Yeo HG, Ahn YJ, Kim K, et al. 2019. Abnormal mitochondria in a non-human primate model of MPTP-induced Parkinson's disease: Drp1 and CDK5/p25 signaling. Exp Neurobiol 28(3):414–424, PMID: 31308800, https://doi.org/10.5607/en.2019.28.3.414.
64. Bröer A, Brookes N, Ganapathy V, Dimmer KS, Wagner CA, Lang F, et al. 1999. The astroglial ASCT2 amino acid transporter as a mediator of glutamine efflux. J Neurochem 73(5):2184–2194, PMID: 10537079.
65. Reddy PH, Reddy TP, Manczak M, Calkins MJ, Shirendeb U, Mao P. 2011. Dynamin-related protein 1 and mitochondrial fragmentation in neurodegenerative diseases. Brain Res Rev 67(1–2):103–118, PMID: 21145355, https://doi.org/10.1016/j.brainresrev.2010.11.004.
66. Betarbet R, Sherer TB, MacKenzie G, Garcia-Osuna M, Panov AV, Greenamyre JT. 2000. Chronic systemic pesticide exposure reproduces features of Parkinson's disease. Nat Neurosci 3(12):1301–1306, PMID: 11100151, https://doi.org/10.1038/81834.
67. Chowdhury AR, Zielonka J, Kalyanaraman B, Hartley RC, Murphy MP, Avadhani NG. 2020. Mitochondria-targeted paraquat and metformin mediate ROS production to induce multiple pathways of retrograde signaling: a dose-dependent phenomenon. Redox Biol 36:101606, PMID: 32604037, https://doi.org/10.1016/j.redox.2020.101606.
68. Cagin U, Duncan OF, Gatt AP, Dionne MS, Sweeney ST, Bateman JM. 2015. Mitochondrial retrograde signaling regulates neuronal function. Proc Natl Acad Sci U S A 112(44):E6000–E6009, PMID: 26489648, https://doi.org/10.1073/pnas.1505036112.
69. Weidling IW, Swerdlow RH. 2020. Mitochondria in Alzheimer's disease and their potential role in Alzheimer's proteostasis. Exp Neurol 330:113321, PMID: 32339611, https://doi.org/10.1016/j.expneurol.2020.113321.
70. Gottlieb RA, Bernstein D. 2016. Mitochondrial remodeling: rearranging, recycling, and reprogramming. Cell Calcium 60(2):88–101, PMID: 27130902, https://doi.org/10.1016/j.ceca.2016.04.006.
71. Butow RA, Avadhani NG. 2004. Mitochondrial signaling: the retrograde response. Mol Cell 14(1):1–15, PMID: 15068799, https://doi.org/10.1016/S1097-2765(04)00179-0.
72. Jazwinski SM. 2013. The retrograde response: when mitochondrial quality control is not enough. Biochim Biophys Acta 1833(2):400–409, PMID: 22374136, https://doi.org/10.1016/j.bbamcr.2012.02.010.
73. Xu F, Armstrong R, Urrego D, Qazzaz M, Pehar M, Armstrong JN, et al. 2016. The mitochondrial division inhibitor Mdivi-1 rescues mammalian neurons from anesthetic-induced cytotoxicity. Mol Brain 9:35, PMID: 27009068, https://doi.org/10.1186/s13041-016-0210-x.
74. Ko AR, Hyun HW, Min SJ, Kim JE. 2016. The differential DRP1 phosphorylation and mitochondrial dynamics in the regional specific astroglial death induced by status epilepticus. Front Cell Neurosci 10:124, PMID: 27242436, https://doi.org/10.3389/fncel.2016.00124.
75. Bordt EA, Clerc P, Roelofs BA, Saladino AJ, Tretter L, Adam-Vizi V, et al. 2017. The putative Drp1 inhibitor mdivi-1 is a reversible mitochondrial complex I inhibitor that modulates reactive oxygen species. Dev Cell 40(6):583–594, PMID: 28350990, https://doi.org/10.1016/j.devcel.2017.02.020.